DOI: 10.1002/chem.200600471

Atoms-in-Molecules Analysis of Extended Hypervalent Five-Center, Six-Electron (5c–6e) C_2Z_2O Interactions at the 1,8,9-Positions of Anthraquinone and 9-Methoxyanthracene Systems

Waro Nakanishi,*[a] Takashi Nakamoto,[a] Satoko Hayashi,[a] Takahiro Sasamori,[b] and Norihiro Tokitoh[b]

Abstract: To clarify the nature of five-center, six-electron (5c–6e) C_2Z_2O interactions, atoms-in-molecules (AIM) analysis has been applied to an anthraquinone, 1,8-$(MeZ)_2$ATQ (**1** (Z=Se), **2** (Z=S), and **3** (Z=O)), and a 9-methoxyanthracene system, 9-MeO-1,8-$(MeZ)_2$ATC (**4** (Z=Se), **5** (Z=S), and **6** (Z=O)), as well as 1-(MeZ)ATQ (**7** (Z=Se), **8** (Z=S), and **9** (Z=O)) and 9-MeO-1-(MeZ)ATC (**10** (Z=Se), **11** (Z=S), and **12** (Z=O)). The total electronic energy density ($H_b(r_c)$) at the bond critical points (BCPs), an appropriate index for weak interactions, has been examined for 5c–6e C_2Z_2O and 3c–4e CZO interactions of the $n_p(O)\cdots\sigma^*(Z-C)$ type in **1**–**12**. Some hydrogen-bonded adducts were also re-examined for convenience of comparison. The total electronic energy densities varied in the following order: O···O (**3**: $H_b(r_c)=0.0028$ au) = O···O (**6**: 0.0028 au) > O···O (**9**: 0.0025 au) ≥ NN···HF (0.0024 au) ≥ O···O (**12**: 0.0023 au) ≫ H_2O···HOH (0.0015 au) > S···O (**8**: 0.0013 au) = S···O (**2**: 0.0013 au) ≥ S···O (**11**: 0.0012 au) = S···O (**5**: 0.0012 au) > HF···HF (0.0008 au) = Se···O (**10**: 0.0008 au) = Se···O (**4**: 0.0008 au) ≥ Se···O (**1**: 0.0007 au) ≥ Se···O (**7**: 0.0006 au) ≫ HCN···HF (−0.0013 au). $H_b(r_c)$ values for S···O were predicted to be smaller than the hydrogen bond of H_2O···HOH and $H_b(r_c)$ values for Se···O are very close to or slightly smaller than that for HF···HF in both the ATQ and 9-MeOATC systems. In the case of Z=Se and S, $H_b(r_c)$ values for 5c–6e C_2Z_2O interactions are essentially equal to those for 3c–4e CZO if Z is the same. The results demonstrate that two $n_p(O)\cdots\sigma^*(Z-C)$ 3c–4e interactions effectively connect through the central $n_p(O)$ orbital to form the extended hypervalent 5c–6e system of the $\sigma^*(C-Z)\cdots n_p(O)\cdots\sigma^*(Z-C)$ type for Z=Se and S in both systems. Natural bond orbital (NBO) analysis revealed that $n_s(O)$ also contributes to some extent. The electron charge densities at the BCPs, NBO analysis, and the total energies calculated for **1**–**12**, together with the structural changes in the PhSe derivatives, support the above discussion.

Keywords: ab initio calculations · anthracenes · atoms-in-molecules (AIM) theory · chalcogens · hypervalent compounds

Introduction

Extended hypervalent bonds, *m*c–*n*e ($m \geq 4$),[1–4], which are σ-type linear bonds that are greater than three-center, four-electron bonds (3c–4e), are of current interest.[1d,5–8] Our strategy to construct *m*c–*n*e ($m \geq 4$) bonds is to employ non-bonded interactions containing lone-pair orbitals.[2–4] We have previously reported the formation of extended hypervalent 4c–6e Z_4 (Z=Se, S, and Br),[2,4] 5c–6e C_2Z_2O (Z=Se and S),[3] 6c–8e Se_2Br_4, and 7c–10e Se_2Br_5 bonds,[4] as well as their nature. Linear alignments of four atoms have also been reported by others, although they are not recognized as extended hypervalent bonds.[9] Weak interactions control the fine structures of compounds and create highly functionalized materials. Information on the weak interactions will also be supplied through the elucidation of the nature of extended hypervalent *m*c–*n*e ($m \geq 4$) bonds.

The formation of 5c–6e C_2Z_2O systems was established on the basis of the linear alignment of five C–Z···O···Z–C

[a] Prof. Dr. W. Nakanishi, T. Nakamoto, Dr. S. Hayashi
Department of Materials Science and Chemistry
Faculty of Systems Engineering, Wakayama University
930 Sakaedani, Wakayama 640-8510 (Japan)
Fax: (+81) 73-457-8253
E-mail: nakanisi@sys.wakayama-u.ac.jp

[b] Dr. T. Sasamori, Prof. Dr. N. Tokitoh
Institute for Chemical Research, Kyoto University
Uji, Kyoto 611-0011 (Japan)

Supporting information for this article is available on the WWW under http://www.chemeurj.org/ or from the author.

 © 2007 Wiley-VCH Verlag GmbH & Co. KGaA, Weinheim

atoms (Z = Se and S) in 1,8-bis(phenylselanyl)anthraquinone (**I**), 9-methoxy-1,8-bis(phenylselanyl)anthracene (**II**), and their derivatives. The quantum chemical (QC) calculations, incorporating the energy-lowering effect of linear alignment, the direction of the charge transfer (CT), and the orbital interaction maps, support the formation of 5c–6e C_2Z_2O in **I** and **II**. The linear alignment of the 5c–6e C_2Z_2O entity is a typical example of an extended hypervalent bond.[3] Scheme 1 shows the molecular orbital approximation of 5c–6e Z_5. Indeed, the simple bonding scheme enables us to visualize how molecular orbitals are constructed from the atomic orbitals in 5c–6e Z_5, but it never provides information on the nature of the bonding. We were very interested in the real nature of the bonding in 5c–6e C_2Z_2O. However, the nature of the bonding between the oxygen and chalcogen atoms in 5c–6e C–Z···O···Z–C (Z = Se and S) has not been clarified yet.

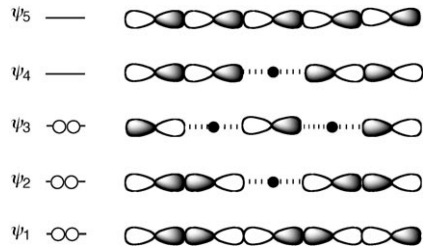

Scheme 1. Molecular orbital approximation of 5c–6e Z_5.

Bader proposed a method to analyze chemical bonds, as well as their nature, that is known as the AIM (atoms-in-molecules) method.[10] The method can be applied to weak bonds as well as classical chemical bonds.[11–16] Some criteria have been proposed to enable weak interactions to be recognized, separate from the classical bonds, based on the nature of the bond critical points (BCPs).[10]

We applied the AIM method to the extended hypervalent 5c–6e C_2Z_2O (Z = Se, S, and O) unit in the anthraquinone (ATQ) system, 1,8-bis(methylchalcogeno)anthraquinones (1,8-$(MeZ)_2$ATQ: **1** (Z = Se), **2** (Z = S), and **3** (Z = O)) after determination of the structures by means of X-ray crystallographic analysis. Of plausible structures such as **AA** and **BB**, compounds **1**–**3** adopt the **BB** structure, according to our definition, with both Z–C_{Me} bonds lying in the ATQ plane, similar to the cases of **I** and **II** (Scheme 2). p–π conjugation

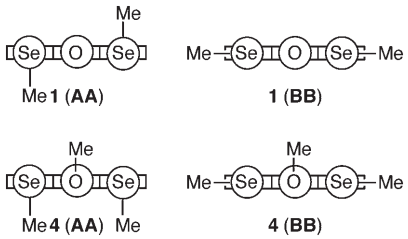

Scheme 2. **AA** and **BB** structures in **1** and **4**.

of the $n_p(Z)$–π(ATQ)–$n_p(Z)$ type must play an important role in stabilizing 5c–6e C_2Z_2O (**BB**). No such p–π conjugation is present in the 9-methoxyanthracene (9-MeOATC) system, 9-methoxy-1,8-bis(methylchalcogeno)anthracenes (9-MeO-1,8-$(MeZ)_2$ATC: **4** (Z = Se), **5** (Z = S), and **6** (Z = O)), owing to the lack of a suitable $n_p(O)$ orbital. Therefore, the purer 5c–6e C_2Z_2O nature will be clarified by examining the bonding nature in **4**–**6**. AIM analysis was also applied to **4**–**6**. Scheme 3 shows how extended hypervalent 5c–6e

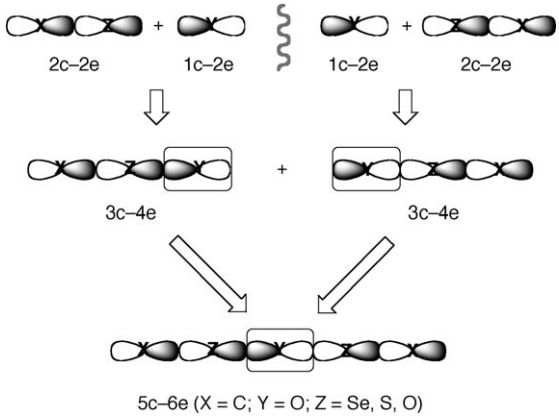

Scheme 3. Formation of 5c–6e X_2Z_2Y through the connection of two 3c–4e XZY entities through the central $n_p(Y)$ orbital.

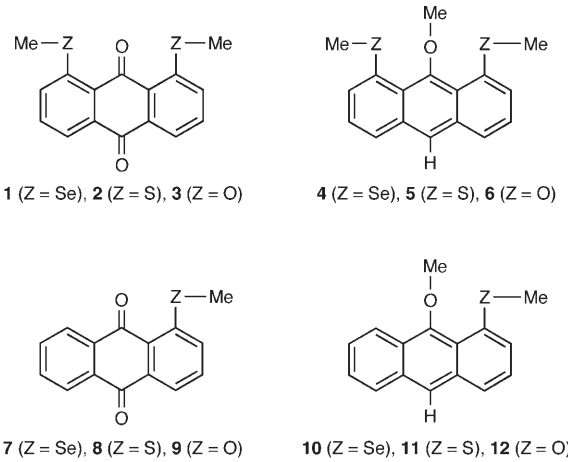

C_2Z_2O interactions of the σ*(C–Z)···$n_p(O)$···σ*(Z–C) type can be formed starting from two hypervalent 3c–4e interactions of the $n_p(O)$···σ*(Z–C) type, connecting effectively through the central $n_p(O)$ orbital. AIM analysis was also carried out for the 3c–4e O···Z–C interactions in 1-(MeZ)ATQ (**7** (Z = Se), **8** (Z = S), and **9** (Z = O)) and 9-MeO-1-(MeZ)ATC (**10** (Z = Se), **11** (Z = S), and **12** (Z = O)) for convenience of comparison.

Herein, we report the results of the AIM analysis of 5c–6e C_2Z_2O in **1**–**6**, as well as 3c–4e CZO in **7**–**12**, which clarifies the nature of the bonds. To the best of our knowledge this is the first AIM treatment of extended hypervalent

 © 2007 Wiley-VCH Verlag GmbH & Co. KGaA, Weinheim

bonds. The contribution of CT to 5c–6e C_2Z_2O in **1**–**6** and 3c–4e CZO interactions in **7**–**12** has also been evaluated by using natural bond orbital (NBO) analysis. The results demonstrate that the CT in 5c–6e C_2Z_2O in **1**–**6** and 3c–4e CZO in **7**–**12** controls the total energies. The results confirm that the energy-lowering effect is responsible for the formation of extended hypervalent bonds.

Results and Discussion

Structures of 1,8-(MeZ)$_2$ATQ (Z = Se, S, and O: 1–3): The X-ray crystallographic analysis was carried out on suitable single crystals of **1**–**3**, which were obtained by slow evaporation of solutions of the compounds in benzene containing 10–30% v/v ethanol. Crystals of **1** and **3** contain only one type of structure, whereas crystals of **2** contain two types of structures (**2** (S-A) and **2** (S-B)). The crystallographic data is collected in Table 1 and selected interatomic distances, angles, and torsional angles are reported in Table 2. Figures 1, 2, and 3 show the structures of **1**, **2** (S-A), and **3**, respectively. The structure of **2** (S-B) is given in the Supporting Information.

Table 2. Selected interatomic distances [Å], angles [°], and torsional angles [°] in **1**–**3**.

	1	**2** (S-A)	**2** (S-B)	**3**[a]
interatomic distances				
Z(1)–O(1)	2.6356(13)	2.6364(11)	2.6495(11)	2.6169(15)
Z(2)–O(1)	2.6344(13)	2.6485(11)	2.6392(11)	2.6129(15)
Z(1)–C(1)	1.9100(19)	1.7631(14)	1.7610(14)	1.3590(16)
Z(1)–C(15)	1.950(2)	1.8055(15)	1.8063(15)	1.4357(17)
Z(2)–C(11)	1.9176(19)	1.7642(14)	1.7655(14)	1.3565(16)
Z(2)–C(16)	1.955(2)	1.8085(15)	1.8119(15)	1.4334(17)
O(1)–C(13)	1.233(2)	1.2266(17)	1.2296(17)	1.2209(17)
angles				
Z(1)-O(1)-Z(2)	150.72(6)	158.21(4)	157.97(4)	150.15(6)
C(1)-Z(1)-C(15)	100.19(8)	102.43(7)	102.67(7)	117.90(11)
C(11)-Z(2)-C(16)	99.68(9)	102.83(7)	102.71(7)	118.19(11)
O(1)-Z(1)-C(15)	174.68(7)	179.75(7)	178.49(5)	155.05(9)
O(1)-Z(2)-C(16)	174.33(7)	176.08(6)	171.98(6)	151.15(9)
C(12)-C(13)-O(1)	120.25(16)	120.07(12)	120.24(12)	121.39(13)
C(14)-C(13)-O(1)	119.70(16)	120.10(12)	119.99(12)	120.44(12)
C(14)-C(1)-Z(1)	120.80(13)	120.95(10)	121.06(10)	117.57(12)
C(12)-C(11)-Z(2)	120.43(13)	121.36(10)	120.97(10)	117.83(12)
C(2)-C(1)-Z(1)	120.70(14)	120.47(11)	120.51(11)	122.57(12)
C(10)-C(11)-Z(2)	120.79(14)	120.86(11)	120.91(11)	122.26(12)
torsional angles				
C(15)-Z(1)-C(1)-C(14)	175.74(15)	178.72(11)	177.66(11)	168.01(12)
C(16)-Z(2)-C(11)-C(12)	−178.42(15)	−173.14(11)	170.27(11)	177.92(12)
O(1)-C(13)-C(14)-C(5)	−177.73(17)	−177.62(12)	175.31(12)	−159.35(14)
O(1)-C(13)-C(12)-C(7)	−176.95(17)	177.52(12)	176.10(12)	−161.48(14)
C(6)-C(5)-C(14)-C(1)	−179.53(16)	179.32(12)	179.32(12)	172.96(11)
C(6)-C(7)-C(12)-C(11)	−179.33(16)	−179.10(12)	−179.54(12)	−177.95(11)
C(6)-C(5)-C(14)-C(13)	1.7(3)	−0.50(19)	0.69(19)	−10.82(19)
C(6)-C(7)-C(12)-C(13)	−0.1(3)	0.70(18)	0.87(19)	6.44(19)

[a] Z(1) and Z(2) are O(3) and O(4), respectively.

The structures of **1**, **2** (S-A), and **2** (S-B) are very close to C_{2v} symmetry, although the oxygen atom at the 9-position flips slightly from the ATQ plane in each molecule. The structure of **3** is rather close to C_s symmetry, with the oxygen atom at the 9-position flipping from the ATQ plane and the MeO groups moving in the opposite directions from the plane, although the magnitudes are not the same. The structures around the Z atoms in **1**–**3** are all **BB** by our definition, with the Z–C_{Me} bonds in the ATQ plane (Figures 1, 2, and 3; see also Scheme 2).[3,17] The planarity of the anthraquinonyl group, containing the Z–C_{Me} bonds, is very good for **1** and **2**, but the structure is slightly bent in **3**, as shown in Figures 1, 2, and 3 and by the data in Table 2.

The nonbonded O(1)···Se(1) and O(1)···Se(2) distances in **1** are 2.6356(13) and 2.6344(13) Å, respectively, which are 0.78–0.79 Å shorter

Table 1. Crystallographic data for **1**–**3**.

	1	**2**	**3**
formula	$C_{16}H_{12}O_2Se_2$	$C_{16}H_{12}O_2S_2$	$C_{16}H_{12}O_4$
M_r	394.18	300.38	268.26
T [K]	103(2)	103(2)	103(2)
crystal system	monoclinic	monoclinic	monoclinic
space group	$P2_1/c$ (no. 14)	$P12_1/n1$ (no. 14)	$P2_1/a$ (no. 14)
a [Å]	9.332(2)	14.171(3)	12.6272(12)
b [Å]	15.862(4)	12.058(2)	6.6216(4)
c [Å]	9.451(2)	16.221(3)	15.6593(14)
β [°]	107.483(3)	111.3621(19)	112.844(4)
V [Å^3]	1334.3(6)	2581.3(9)	1206.61(17)
Z	4	8	4
ρ_{calcd} [g cm^{-3}]	1.962	1.546	1.477
F(000)	768	1248	560
no. of reflections collected	8865	22316	8103
no. of independent reflections	2479 (R_{int} = 0.0199)	5021 (R_{int} = 0.0141)	2352 (R_{int} = 0.0193)
no. of data/restraints/params	2479/0/229	5021/0/457	2352/0/229
goodness of fit, F_2	1.081	1.118	1.113
R_1, wR_2	0.0177, 0.0422 [I>2.0σ(I)]	0.0300, 0.0853 [I>2.0σ(I)]	0.0403, 0.0990 [I>2.0σ(I)]
largest diff. peak [e Å^{-3}]	0.371 to −0.422	0.420 to −0.229	0.420 to −0.279

© 2007 Wiley-VCH Verlag GmbH & Co. KGaA, Weinheim

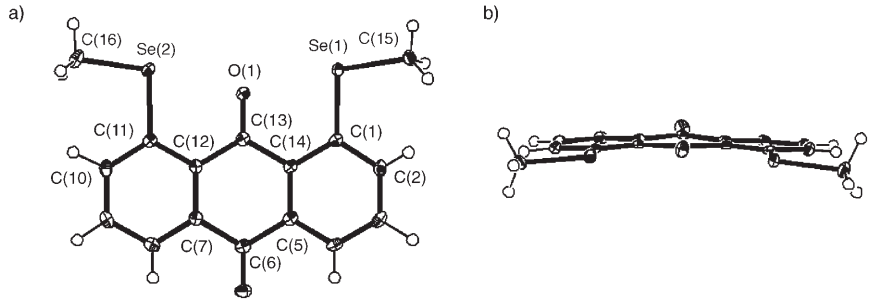

Figure 1. Structure of **1**: a) side view and b) top view (thermal ellipsoids are shown at the 50% probability level).

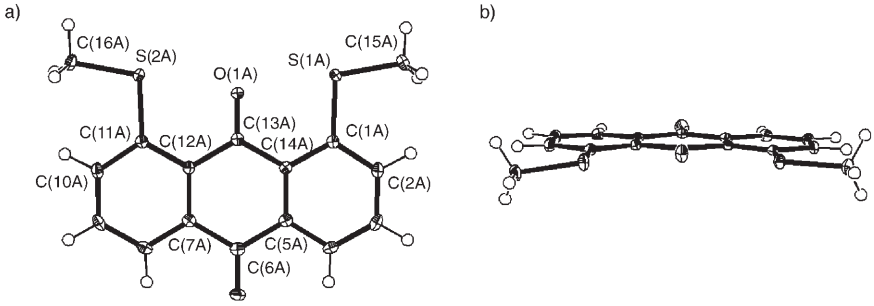

Figure 2. Structure of **2** (S-A): a) side view and b) top view (thermal ellipsoids are shown at the 50% probability level).

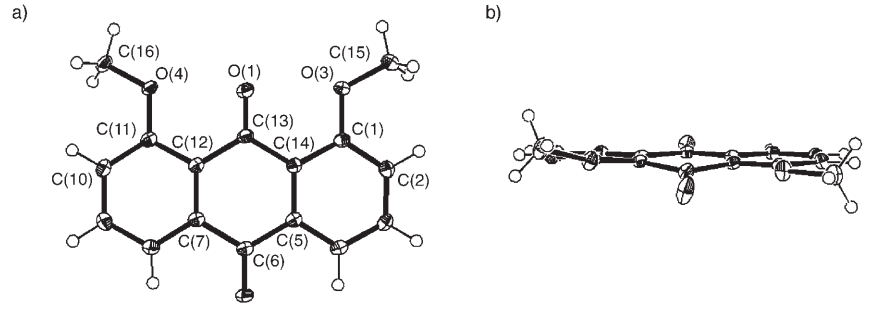

Figure 3. Structure of **3**: a) side view and b) top view (thermal ellipsoids are shown at the 50% probability level).

than the sum of the van der Waals radii of the atoms (3.42 Å).[18] The O(1)-Se(1)-C(15) and O(1)-Se(2)-C(16) angles are 174.68(7) and 174.33(7)°, respectively, which are close to 180° and desirable for the formation of a linear bond. The Se(1)-O(1)-Se(2) angle is 150.72(6)°, which is a deviation of about 30° from 180°. The angle is mainly determined by the O(1)−C(13), Se(1)−C(1), and Se(2)−C(11) distances, as well as the angles around the atoms. If nonbonded 3c–4e $n_p(O)\cdots\sigma^*(Se-C)$-type interactions occur on both sides of the central $n_p(O)$ orbital and the two interactions are connected effectively through the common $n_p(O)$ orbital, the resulting nonbonded $\sigma^*(C-Se)\cdots n_p(O)\cdots\sigma^*(Se-C)$ interaction leads to the formation of the 5c–6e C_2Se_2O system. Indeed, a 30° deviation of ∢Se(1)O(1)Se(2) would be borderline for the formation of the linear bond, but the central p_x orbital at the O(1) atom will work to form a 5c–6e system because the deviation is around 15° on each side of the p_x orbital if the Se···Se direction is set to the *x* axis.

The nonbonded O···S distances in **2** (S-A) are 2.6364(11) and 2.6485(11) Å,[19] which are 0.67–0.68 Å shorter than the sum of the van der Waals radii of the atoms (3.32 Å).[18] The O(1A)-S(1A)-C(15A) and O(1A)-S(2A)-C(16A) angles for **2** (S-A) are 179.75(7) and 176.08(6)°, respectively,[19] which are close to 180° and desirable for the formation of a linear bond. The S(1A)-O(1A)-S(2A) angle for **2** (S-A) is 158.21(4)°,[19] which is more suitable for the central p_x orbital at the O(1) atom to form a linear 5c–6e C_2S_2O system than is the case of **1**.

In the case of **3**, the O(1)···O(3) and O(1)···O(4) nonbonded distances are 2.6169(15) and 2.6129(15) Å, which are 0.42–0.43 Å shorter than the sum of the van der Waals radii of the atoms (3.04 Å).[18] The O(1)-O(3)-C(15), O(1)-O(4)-C(16), and O(3)-O(1)-O(4) angles are 155.05(9), 151.15(9), and 150.15(6)°, respectively, which deviate from 180° by about 30°. The deviations of all three angles are borderline for the formation of the 5c–6e C_2O_2O system in **3**. Similarly, the O···O nonbonded distances of 2.613–2.617 Å would also be borderline for the interaction. Therefore, the 5c–6e C_2O_2O interaction would be weak in **3**, even if it forms.

AIM analysis: The **BB** forms observed for **1**–**3**[3,17] must be more stable than the **AA** forms; the $Z-C_{Me}$ bonds are in the ATQ plane in **BB** and are almost perpendicular to the plane in **AA** (Scheme 2). The structures of **1**–**3** were optimized by employing the Gaussian 03 program[20] with the 6-311+G(2df) basis set for the oxygen and Z (Z=Se, S, and O) atoms and the 6-311+G(2d,p) basis set for the carbon and hydrogen atoms. Calculations were performed at the density functional theory (DFT) level of the Becke three-parameter

 © 2007 Wiley-VCH Verlag GmbH & Co. KGaA, Weinheim

hybrid functionals with the Lee–Yang–Parr correlation functional (B3LYP). The **BB** forms of **1–3** were optimized as the global minima, which reproduce well the observed structures of **1–3**. The **AA** forms are local ones. The structures of **AA** and **BB** in **4–6** and **A** and **B** in **7–12** were also optimized by using the method applied to **1–3**.

AIM analysis was performed by applying the AIM2000 program[21] to the optimized **BB** structures of **1–6** and **B** structures of **7–12** using the Gaussian 03 program. Table 3 shows the results of the AIM analysis, giving the electron charge density and the total electronic energy density at the BCP between the Z and oxygen atoms ($\rho_b(r_c)$ and $H_b(r_c)$, respectively). Table 3 also gives the natural charges at the Z and oxygen atoms (Qn(Z) and Qn(O), respectively), calculated by the natural population analysis.[22] Figures 4 and 5 exhibit BCPs, bond paths, and the contour maps of $\rho_b(r_c)$ drawn on the optimized structures of **1** and **4**, respectively. Table 4 summarizes some of the data relating to the BCPs of the weak interactions reported in this work.[10a,11,13a] Table 4 also gives data recalculated by a method similar to that used in this work, using the 6-311++G(2df,2p) basis set at the B3LYP and/or MP2 levels, for convenience of comparison.[23] The values recalculated with the B3LYP/6-311++G(2df,2p) method were employed to gain a better understanding of the nature of the interactions.

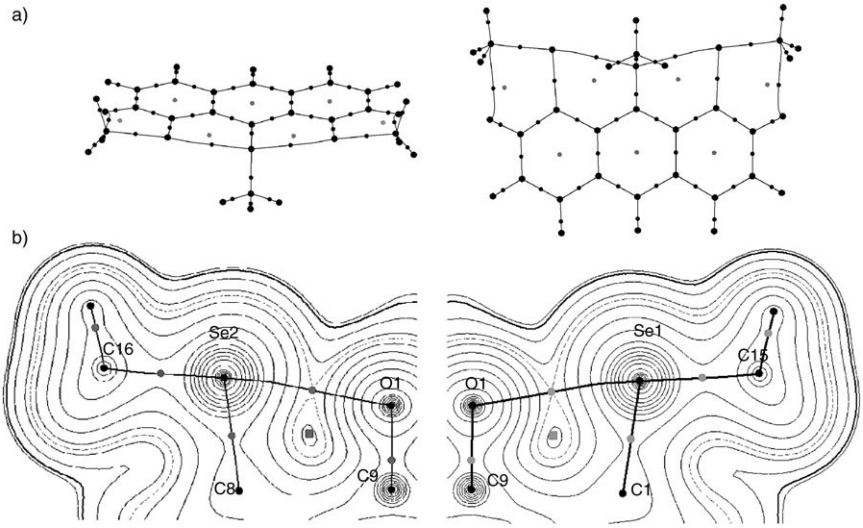

Figure 5. a) BCPs (●), ring critical points (■), and bond paths of **4** and b) the partial contour map of $\rho_b(r_c)$ of **4** in the O_1-Se_2-C_9 and O_1-Se_1-C_9 planes. The contours [$e\,a_o^{-3}$] are at 2^l ($l=\pm8, \pm7, \ldots0$), 0.3028, 0.0216 (dotted line), and 0.0047 (heavy line).

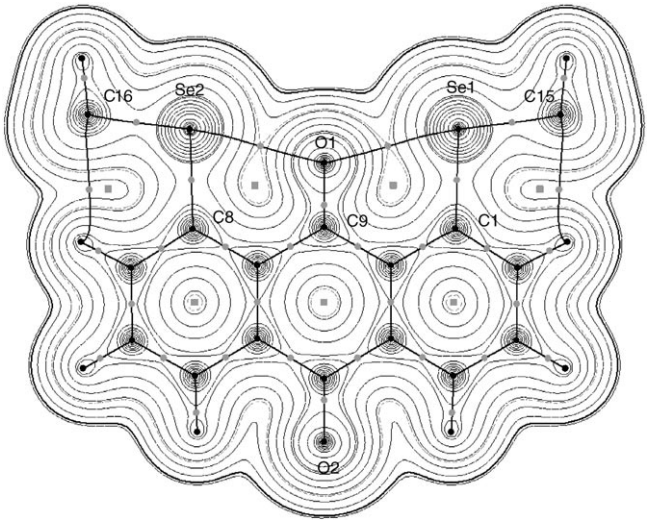

Figure 4. Contour map of $\rho_b(r_c)$ of **1** in the anthraquinone plane, together with BCPs (●), ring critical points (■), and bond paths. The contours [$e\,a_o^{-3}$] are at 2^l ($l=\pm8, \pm7, \ldots0$), 0.3028, 0.0269 (dotted line), and 0.0047 (heavy line).

Before discussing the results for the 5c–6e C_2Z_2O interactions in **1–6**, it may be instructive to start with a discussion of the 3c–4e CZO interactions in **7–12**.

AIM analysis of 3c–4e CZO in 7–12 with $\rho_b(r_c)$: The charge densities at the BCP ($\rho_b(r_c)$) between the nonbonded Z···O atoms in **7** (Z=Se) and **8** (Z=S) of the ATQ system were evaluated to be 0.027 and 0.025 $e\,a_o^{-3}$ ($a_o=0.52177$ Å), respectively (Table 3). While the $\rho_b(r_c)$ values for **7** and **8** are smaller than that for HCN···HF (0.034 $e\,a_o^{-3}$), they are larger than those for H_2O···HOH (0.024 $e\,a_o^{-3}$) and HF···HF (0.025 $e\,a_o^{-3}$), although the $\rho_b(r_c)$ value for **8** is essentially equal to the latter (Table 4).[10a] The results suggest that the Z···O interactions in **7** (Z=Se) and **8** (Z=S) are stronger than the hydrogen bond in H_2O···HOH (and HF···HF), but weaker than the bond in HCN···HF.[10a] The values for **10** (Z=Se) and **11** (Z=S) of the 9-MeOATC system are 0.022 and 0.021 $e\,a_o^{-3}$, respectively (Table 3), which are smaller than that for H_2O···HOH, but larger than that for NN···HF (0.018 $e\,a_o^{-3}$) (Table 4).[10a] The Z···O interactions in **10** (Z=Se) and **11** (Z=S) are substantially stronger than the hydrogen bond in NN···HF, but weaker than the hydrogen bond in H_2O···HOH.[10a] In the case of Z=O, the $\rho_b(r_c)$ values for **9** and **12** are 0.017 and 0.018 $e\,a_o^{-3}$, respectively. These values are slightly smaller than that for NN···HF, but are apparently larger than those corresponding to the van der Waals interactions in Ne···HF and Ar···HF ($\rho_b(r_c)=0.006$ and 0.008 $e\,a_o^{-3}$, respectively) (Table 4).[10a] The results are summarized in Equation (1).

 © 2007 Wiley-VCH Verlag GmbH & Co. KGaA, Weinheim

Table 3. Results of the AIM analysis of the nonbonded Z···O interactions in **1**–**12**.[a]

Compound	BCP in (A, B)	Distance [Å]			$\rho_b(r_c)$ [$e\,a_o^{-3}$]	$\nabla^2\rho_b(r_c)$ [$e\,a_o^{-5}$]	Hessian eigenvalue					$H_b(r_c)$ [au]	Qn(A)	Qn(B)
		r(A, B)	r(A, BCP)	r(B, BCP)			λ_1	λ_2	λ_3	λ_1/λ_2-1	$\lvert\lambda_1\rvert/\lambda_3$			
1	(Se, O)	2.6493	1.3901	1.2611	0.0268	0.0846	−0.0228	−0.0210	0.1284	0.0857	0.178	0.0007	0.4837	−0.6232
	(Se, C)	1.9198	0.9827	0.9372	0.1565	−0.1336	−0.2206	−0.1796	0.2666	0.2283	0.827	−0.0965	0.4837	−0.2404
	(C, O)	1.2312	0.4193	0.8120	0.4012	−0.3659	−1.0633	−0.9931	1.6906	0.0707	0.629	−0.7034	0.6560	−0.6232
2	(S, O)	2.6258	1.3660	1.2685	0.0255	0.0856	−0.0216	−0.0202	0.1275	0.0693	0.169	0.0013	0.3822	−0.6050
	(S, C)	1.7724	0.9136	0.8589	0.1935	−0.2942	−0.3102	−0.2524	0.2685	0.2290	1.155	−0.1311	0.3822	−0.1404
	(C, O)	1.2267	0.4180	0.8087	0.4062	−0.3623	−1.0856	−1.0077	1.7310	0.0773	0.627	−0.7159	0.6721	−0.6050
3	(O, O)	2.5775	1.2668	1.3145	0.0181	0.0803	−0.0165	−0.0158	0.1125	0.0443	0.147	0.0028	−0.5095	−0.5567
	(O, C)	1.3454	0.8859	0.4606	0.3039	−0.5446	−0.6831	−0.6535	0.7920	0.0453	0.863	−0.4675	−0.5095	0.3878
	(C, O)	1.2145	0.4145	0.8000	0.4184	−0.3357	−1.1371	−1.0376	1.8390	0.0959	0.618	−0.7472	0.6538	−0.5567
4	(Se, O)	2.7651	1.4590	1.3095	0.0216	0.0690	−0.0174	−0.0164	0.1027	0.0610	0.169	0.0008	0.4120	−0.5901
	(Se, C)	1.9350	0.9989	0.9361	0.1524	−0.1312	−0.2127	−0.1760	0.2575	0.2085	0.826	−0.0906	0.4120	−0.1742
	(C, O)	1.3757	0.4776	0.8988	0.2869	−0.6090	−0.6091	−0.6003	0.6003	0.0147	1.015	−0.4238	0.3816	−0.5901
5	(S, O)	2.7137	1.4210	1.3047	0.0216	0.0724	−0.0178	−0.0167	0.1069	0.0659	0.167	0.0012	0.3207	−0.5889
	(S, C)	1.7847	0.9291	0.8558	0.1889	−0.2757	−0.3004	−0.2482	0.2728	0.2103	1.101	−0.1236	0.3207	−0.1376
	(C, O)	1.3713	0.4761	0.8959	0.2904	−0.6227	−0.6226	−0.6133	0.6132	0.0152	1.015	−0.4316	0.3841	−0.5889
6	(O, O)	2.5783	1.2715	1.3110	0.0182	0.0805	−0.0165	−0.0162	0.1132	0.0185	0.146	0.0028	−0.5357	−0.5958
	(O, C)	1.3572	0.8928	0.4653	0.2947	−0.5330	−0.6486	−0.6175	0.7332	0.0504	0.885	−0.4465	−0.5357	0.3777
	(C, O)	1.3638	0.4759	0.8889	0.2971	−0.6772	−0.6509	−0.6412	0.6149	0.0151	1.059	−0.4452	0.5276	−0.5958
7	(Se, O)	2.6518	1.3904	1.2633	0.0269	0.0843	−0.0229	−0.0211	0.1283	0.0853	0.178	0.0006	0.4928	−0.5645
	(Se, C)	1.9189	0.9821	0.9369	0.1568	−0.1341	−0.2210	−0.1800	0.2669	0.2278	0.828	−0.0969	0.4928	−0.1737
	(C, O)	1.2250	0.4174	0.8076	0.4073	−0.3485	−1.0870	−1.0144	1.7529	0.0716	0.620	−0.7187	0.5517	−0.5645
8	(S, O)	2.6398	1.3733	1.2753	0.0249	0.0834	−0.0211	−0.0197	0.1242	0.0711	0.170	0.0013	0.3854	−0.5582
	(S, C)	1.7713	0.9128	0.8586	0.1938	−0.2953	−0.3108	−0.2529	0.2684	0.2289	1.158	−0.1317	0.3854	−0.1318
	(C, O)	1.2226	0.4167	0.8059	0.4099	−0.3460	−1.0982	−1.0218	1.7740	0.0748	0.619	−0.7253	0.5507	−0.5582
9	(O, O)	2.6119	1.2849	1.3310	0.0168	0.0733	−0.0150	−0.0140	0.1023	0.0714	0.147	0.0025	−0.5086	−0.5400
	(O, C)	1.3440	0.8851	0.4599	0.3049	−0.5434	−0.6862	−0.6577	0.8005	0.0433	0.857	−0.4698	−0.5086	0.3945
	(C, O)	1.2169	0.4151	0.8018	0.4156	−0.3332	−1.1221	−1.0356	1.8245	0.0835	0.615	−0.7400	0.5511	−0.5400
10	(Se, O)	2.7545	1.4522	1.3061	0.0222	0.0700	−0.0182	−0.0168	0.1050	0.0833	0.173	0.0008	0.4112	−0.5882
	(Se, C)	1.9345	0.9989	0.9357	0.1526	−0.1319	−0.2129	−0.1765	0.2575	0.2062	0.827	−0.0806	0.4112	−0.1670
	(C, O)	1.3758	0.4779	0.8989	0.2864	−0.6084	−0.6092	−0.5978	0.5987	0.0191	1.018	−0.4226	0.3791	−0.5882
11	(S, O)	2.7204	1.4243	1.3086	0.0214	0.0711	−0.0178	−0.0166	0.1054	0.0723	0.169	0.0012	0.3187	−0.5884
	(S, C)	1.7844	0.9297	0.8548	0.1891	−0.2758	−0.3004	−0.2488	0.2735	0.2074	1.098	−0.1236	0.3187	−0.1323
	(C, O)	1.3739	0.4774	0.8974	0.2881	−0.6177	−0.6157	−0.6042	0.6022	0.0190	1.022	−0.4262	0.3805	−0.5884
12	(O, O)	2.6304	1.2996	1.3353	0.0164	0.0703	−0.0142	−0.0136	0.0982	0.0441	0.145	0.0023	−0.5383	−0.5811
	(O, C)	1.3576	0.8935	0.4650	0.2943	−0.5259	−0.6465	−0.6157	0.7363	0.0500	0.878	−0.4452	−0.5383	0.3826
	(C, O)	1.3713	0.4782	0.8942	0.2908	−0.6469	−0.6271	−0.6157	0.5959	0.0185	1.052	−0.4310	0.3853	−0.5811

[a] Optimized with 6-311+G(2df) basis set for the oxygen and Z (Se, S, and O) atoms and with the 6-311+G(2d,p) basis set for the carbon and hydrogen atoms at the DFT (B3LYP) level of the Gaussian 03 program.

© 2007 Wiley-VCH Verlag GmbH & Co. KGaA, Weinheim

Table 4. Results of the AIM analysis of weak interactions.

Adducts	BCP (A, B)	Distance [Å] r(A, B)	$\rho_b(r_c)$ [$e\,a_o^{-3}$]	$\nabla^2\rho_b(r_c)$ [$e\,a_o^{-5}$]	Hessian eigenvalue $\lvert\lambda_1\rvert/\lambda_3$	$H_b(r_c)$ [au]	Qn(A)	Qn(B)
van der Waals								
Ne–HF[a,b]	(Ne, H)	2.110	0.0099	0.0484	0.180			
Ne–HF[c,d]	(Ne, H)	2.3211	0.0058	0.0295	0.161	0.0014	0.0009	0.5513
Ar–HF[a,b]	(Ar, H)	2.562	0.0077	0.0311	0.170			
Ar–HF[c,d]	(Ar, H)	2.5573	0.0079	0.0302	0.174	0.0016	0.0031	0.5508
hydrogen bonds								
NN–HF[a,b]	(N, H)	2.076	0.0169	0.0647	0.200			
NN–HF[c,d]	(N, H)	2.0639	0.0175	0.0636	0.209	0.0024	−0.0468	0.5567
$(H_2O)_2$[b,e]	(O, H)	2.039	0.0198	0.0623	0.223			
$(H_2O)_2$[c,f]	(O, H)	1.9521	0.0233	0.0832	0.214	0.0012	−0.9365	0.4854
$(H_2O)_2$[c,d]	(O, H)	1.9576	0.0236	0.0801	0.222	0.0015	−0.9334	0.4831
$(HF)_2$[b,e]	(H, F)	1.778	0.0262	0.1198	0.204			
$(HF)_2$[c,f]	(H, F)	1.8440	0.0233	0.0936	0.213	0.0007	0.5541	−0.5487
$(HF)_2$[c,d]	(H, F)	1.8291	0.0250	0.0939	0.224	0.0008	0.5604	−0.5550
HCN–HF[a,b]	(N, H)	1.881	0.0284	0.0920	0.236			
HCN–HF[c,d]	(N, H)	1.8200	0.0338	0.0944	0.266	−0.0013	−0.3801	0.5649
trihalide linear anions								
$[Br_3]^-$[c,d,g]	(Br, Br)	2.6212	0.0579	0.0668	0.295	−0.0107	−0.1010	−0.4495
$[Cl_3]^-$[g–i]	(Cl, Cl)		0.063	0.117	0.259			
$[Cl_3]^-$[c,d,g]	(Cl, Cl)	2.3459	0.0762	0.0951	0.311	−0.0180	−0.1086	−0.4457
$[F_3]^-$[g–i]	(F, F)		0.100	0.539	0.199			
$[F_3]^-$[c,d,g]	(F, F)	1.7275	0.1099	0.5404	0.217	−0.0060	−0.1018	−0.4491
13 (C_{2v})[j,k]	(B, O)	2.431	0.022	0.058	0.266			

[a] With the MP2/6-311G(2d,2p) method of the Gaussian 98 program.[37] [b] See ref. [10a]. [c] Recalculated in this work. [d] With the B3LYP/6-311++G(2df,2p) method of the Gaussian 03 program. [e] With the 6-31G** method of the Gaussian 98 program. [f] With the MP2/6-311++G(2df,2p) method of the Gaussian 03 program. [g] The central atom being called A and the outside ones B. [h] With the 6-311++G** method. [i] See ref. [11]. [j] With the 6-31G(d) method at the DFT (B3PW91) level of the Gaussian 98 program. [k] See ref. [13a].

$$\mathrm{Ar\cdots HF}\ (\rho_b(r_c)=0.008\,e\,a_o^{-3}) \ll \mathrm{O\cdots O}\ (\mathbf{12}:\ 0.016) \leq \mathrm{O\cdots O}\ (\mathbf{9}:\ 0.017) \leq \mathrm{NN\cdots HF}\ (0.018) < \mathrm{S\cdots O}\ (\mathbf{11}:\ 0.021) \leq \mathrm{Se\cdots O}\ (\mathbf{10}:\ 0.022) < \mathrm{H_2O\cdots HOH}\ (0.024) \leq \mathrm{S\cdots O}\ (\mathbf{8}:\ 0.025) = \mathrm{HF\cdots HF}\ (0.025) < \mathrm{Se\cdots O}\ (\mathbf{7}:\ 0.027) \ll \mathrm{HCN\cdots HF}\ (0.034) \quad (1)$$

The $\nabla^2\rho_b(r_c)$ values for **7**–**12** are 0.070–0.084 $e\,a_o^{-5}$ (Table 3). The values lie in the range of hydrogen-bonded adducts (0.064–0.094 $e\,a_o^{-5}$). In general, negative values of $\nabla^2\rho_b(r_c)$ appear at the BCPs of covalent bonds, whereas positive values correspond to ionic bonds.[10] The positive values of $\nabla^2\rho_b(r_c)$ in **7**–**12** are well understood based on this generalization. The ionic nature of the nonbonded Z···O interactions for Z=Se and S are well understood based on the CT of hypervalent $n_p(O)\rightarrow\sigma^*(Z–C)$ 3c–4e interactions. The (Qn(Se), Qn(O)) values are (0.493, −0.565) for **7** and (0.411, −0.588) for **10** and (Qn(S), Qn(O)) are (0.385, −0.558) for **8** and (0.319, −0.588) for **11**.[22] The positive and negative values developed at the chalcogen (Z=Se and S) and oxygen atoms support the ionic nature of the interactions.

The contributions of π character to the C_1–Z bonds of **7**–**12** were examined. The ellipticities of the p–π conjugation of p(Z)–π(ATQ) type in **7** (Z=Se: $\lambda_1/\lambda_2-1=\varepsilon=0.23$) and **8** (Z=S: 0.23) of the ATQ system are larger than those of **10** (Z=Se: $\varepsilon=0.21$) and **11** (Z=S: 0.21) of the 9-MeOATC system. The values are also much larger than those for H_2C=Se ($\varepsilon=0.13$) and H_2C=S ($\varepsilon=0.05$),[12] although the basis sets used for the calculations were not the same. The results show that p–π conjugation is significant in the C_1–Z bonds of **7**, **8**, **10**, and **11**. The values for **9** (Z=O: $\varepsilon=0.04$) and **12** (Z=O: 0.05) are similar to the value of the ellipticity of H_2C=O (0.04).[12,24] The values of the ellipticity in the Z···O interactions in **7** (Z=Se: $\varepsilon=0.09$) and **8** (Z=S: 0.07) are similar to those in **10** (Z=Se: $\varepsilon=0.08$) and **11** (Z=S: 0.07). The magnitude of the π character of the Z···O bonds in **7** and **8** is comparable to that in **10** and **11**, although **10** and **11** seem to have no suitable p orbitals with which to construct the π(Z···O) interactions. The values for the Z···O interactions in **7**, **8**, **10**, and **11** are larger than that for H_2C=S and smaller than that for H_2C=Se.[12] While the ellipticity of the O···O interactions in **9** ($\varepsilon=0.07$) is very close to the values for **8** and **11**, that for **12** (0.04) is smaller.

After elucidation of the nature of the BCPs in **7**–**12**, we extended this study to the BCPs of the 5c–6e C_2Z_2O interactions in **1**–**6**.

AIM analysis of 5c–6e C_2Z_2O in 1–6 with $\rho_b(r_c)$: The optimized structures of **1**–**3** are of C_{2v} symmetry and those of **4**–**6** are of C_s symmetry.[25] Therefore, the nature of the two BCPs in the nonbonded C–Z···O···Z–C interactions in **1**–**6** is the same. One of them is listed in Table 3.

 © 2007 Wiley-VCH Verlag GmbH & Co. KGaA, Weinheim

The $\rho_b(r_c)$ values for the nonbonded C–Z···O···Z–C interactions in **1** (Z=Se) and **2** (Z=S) are 0.027 and 0.026 $e\,a_o^{-3}$, respectively, and those for **4** (Z=Se) and **5** (Z=S) are both 0.022 $e\,a_o^{-3}$. The values of the C–O···O···O–C interactions in **3** and **6** are both 0.018 $e\,a_o^{-3}$. The results for the 5c–6e C_2Z_2O interactions of **1–6** are summarized in Equation (2), along with the data for some hydrogen-bonded adducts.

$$\begin{aligned}&NN\cdots HF\ (\rho_b(r_c)=0.018\,e\,a_o^{-3})=O\cdots O\ (\mathbf{3}:\ 0.018)=\\&O\cdots O\ (\mathbf{6}:\ 0.018)<S\cdots O\ (\mathbf{5}:\ 0.022)=Se\cdots O\ (\mathbf{4}:\\&0.022)<H_2O\cdots HOH\ (0.024)\le HF\cdots HF\ (0.025)\le\\&S\cdots O\ (\mathbf{2}:\ 0.026)\le Se\cdots O\ (\mathbf{1}:\ 0.027)\ll\\&HCN\cdots HF\ (0.034)\end{aligned}\qquad(2)$$

The results show that the values of $\rho_b(r_c)$ for **1** and **2** of the ATQ system are larger than those for H_2O···HOH and HF···HF, whereas those for the 9-MeOATC system with Z= Se and S are smaller than that for H_2O···HOH. The values for the O···O interactions are essentially equal to that for NN···HF.

Equations (1) and (2) were combined to give Equation (3). The characteristics of the 5c–6e C_2Z_2O and 3c–4e CZO interactions of **1–12**, predicted on the basis of the values of $\rho_b(r_c)$, are as follows: $\rho_b(r_c)$ values for 5c–6e Z_2C_2O for Z=Se and S are essentially equal to those for 3c–4e ZCO, respectively, if the system is the same, whereas the former is slightly larger than the latter for Z=O. The results are in accord with the expectation that the Z···O interactions in 5c–6e C_2Z_2O (Z=Se, S, and O) are very similar to those in 3c–4e CZO. No saturation effect was detected in 5c–6e C_2Z_2O, relative to 3c–4e CZO, on the basis of the $\rho_b(r_c)$ values. These results demonstrate that the extended hypervalent 5c–6e interactions in **1–6** of the σ*(C–Z)···n_p(O)···σ*(Z–C) type are formed by connecting two 3c–4e n_p(O)···σ*(Z–C) elements effectively through the central n_p(O) orbital.

$$\begin{aligned}&Ar\cdots HF\ (\rho_b(r_c)=0.008\,e\,a_o^{-3})\ll O\cdots O\ (\mathbf{12}:\ 0.016)\le\\&O\cdots O\ (\mathbf{9}:\ 0.017)\le NN\cdots HF\ (0.018)=O\cdots O\ (\mathbf{3}:\\&0.018)=O\cdots O\ (\mathbf{6}:\ 0.018)<S\cdots O\ (\mathbf{11}:\ 0.021)\le\\&S\cdots O\ (\mathbf{5}:\ 0.022)=Se\cdots O\ (\mathbf{4}:\ 0.022)=Se\cdots O\ (\mathbf{10}:\\&0.022)<H_2O\cdots HOH\ (0.024)\le HF\cdots HF\ (0.025)=\\&S\cdots O\ (\mathbf{8}:\ 0.025)\le S\cdots O\ (\mathbf{2}:\ 0.026)\le Se\cdots O\ (\mathbf{1}:\\&0.027)=Se\cdots O\ (\mathbf{7}:\ 0.027)\ll HCN\cdots HF\ (0.034)\end{aligned}\qquad(3)$$

The π character of the nonbonded Z···O interactions in 5c–6e C_2Z_2O is essentially the same as that in 3c–4e CZO, and so are the C_1–Z and C=O bonds (Table 3).

Yamamoto and co-workers reported the AIM analysis of the O···B···O 3c–4e interactions at the 1,8,9-positions of 9-(1,2-$C_6H_4O_2B$)-1,8-$(MeO)_2C_{14}H_7$ (**13**).[13] The $\rho_b(r_c)$ value is 0.022 $e\,a_o^{-3}$ for the C_{2v} symmetric structure. While the $\rho_b(r_c)$ value for **13** is larger than those for the O···O interactions in **3** and **6**, it is smaller than those for the O···Z (Z= Se and S) interactions in **1**, **4**, **2**, and **5**, although the method of calculation was not the same. Because the conformation around the MeO groups in **13** is **BB**, the n_s(O) orbitals must act as donors in **13**. The conformations around Me–Z (Z=Se, S, and O) in **1–6** are all **BB**, therefore, the n_p(O) orbital of the central oxygen atom will play an important role in **1–6** as the donor. The direction of CT in **1–6** is completely different from that in **13**: CT in **1–6** is of the σ*(C–Z)←n_p(O)→σ*(Z–C) type, whereas that in **13** must be of the n_s(O)→n_p(B)←n_s(O) type.[26,27]

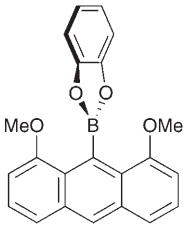

13 (C_{2v})

Linear trihalide ions, X_3^-, are typical examples of 3c–4e interactions. The $\rho_b(r_c)$ values for F_3^-, Cl_3^-, and Br_3^- are 0.110, 0.076, and 0.058 $e\,a_o^{-3}$, respectively (Table 4). These values are about four, three, and two times larger than that of **1**, respectively. The values decrease in the order $F_3^- > Cl_3^- > Br_3^-$. The stability of X_3^- relative to X_2 and X^-, ($\Delta E(X_3^-)=E(X_3^-)-E(X_2)-E(X^-)$) were evaluated to be −142.0, −124.1, and −137.7 kJ mol^{-1}, for X=F, Cl, and Br, respectively. The stabilization energies do not correlate well with $\rho_b(r_c)$, which shows that $\rho_b(r_c)$ does not reflect the stability in some cases.

After examination of the nature of the 5c–6e C_2Z_2O and 3c–4e CZO interactions based mainly on $\rho_b(r_c)$ values, the next step was to employ the total electronic energy density at the BCP ($H_b(r_c)$), which will be a more appropriate index for the weak interactions.

AIM analysis on 5c–6e C_2Z_2O and 3c–4e CZO with $H_b(r_c)$: The total electronic energy density at the BCP ($H_b(r_c)$) is the sum of the electronic potential (V) and kinetic energy (G) densities at the BCP ($H_b(r_c)=G_b(r_c)+V_b(r_c)$).[28] The values of $H_b(r_c)$ for 5c–6e C_2Z_2O and 3c–4e CZO interactions in **1–12** are also collected in Table 3. $G_b(r_c)$ and $V_b(r_c)$ are positive and negative, respectively, although not shown in Table 3. Because the magnitudes of $G_b(r_c)$ are slightly larger than the corresponding $V_b(r_c)$ values, $H_b(r_c)$ values for **1–12** show a slightly positive nature. As also recognized in Table 3, $H_b(r_c)$ values are negative for classical chemical bonds in **1–12**. The values for X_3^- (X=F, Cl, and Br) and HCN···HF are also negative. However, those for the van der Waals and hydrogen-bonded adducts in Table 4 are positive, except in the case of HCN···HF: the positive values of $H_b(r_c)$ correspond to the ionic interactions.[11,12] The $H_b(r_c)$ values for the nonbonded O···Z–C interactions in **1–12** are all positive (Table 3). The $H_b(r_c)$ values will clarify the nature of the interactions.

The values of $H_b(r_c)$ for the nonbonded O···Z–C interactions of **1–12** are summarized in Equation (4), together with those for hydrogen-bonded adducts. The nonbonded O···Z

 © 2007 Wiley-VCH Verlag GmbH & Co. KGaA, Weinheim

interactions are classified into three groups by their $H_b(r_c)$ values. $0.0028 \geq H_b(r_c$: Z=O$) \geq 0.0023$, $0.0013 \geq H_b(r_c$: Z=S$) \geq 0.0012$, and $0.0008 \geq H_b(r_c$: Z=Se$) \geq 0.0006$. Therefore, $H_b(r_c$: Z=O$) \approx H_b(r_c$: NN···HF$)$, $H_b(r_c$: H_2O···HOH$) \geq H_b(r_c$: Z=S$) \geq H_b(r_c$: HF···HF$)$, and $H_b(r_c$: HF···HF$) \geq H_b(r_c$: Z=S$)$. $H_b(r_c)$ values for the O···Z interactions decrease in the order $Z=O \gg S > Se$. It has been demonstrated that the σ*(C–Z)···n_p(O)···σ*(Z–C) 5c–6e interactions are effectively formed by the connection of two n_p(O)···σ*(Z–C) 3c–4e entities through the central n_p(O) orbital, again based on values of $H_b(r_c)$.

$$\begin{aligned}&\mathrm{O\cdots O}\ (\mathbf{3}:\ H_b(r_c) = 0.0028\ \mathrm{au}) = \mathrm{O\cdots O}\ (\mathbf{6}:\ 0.0028) > \\ &\mathrm{O\cdots O}\ (\mathbf{9}:\ 0.0025) \geq \mathrm{NN\cdots HF}\ (0.0024) \geq \mathrm{O\cdots O}\ (\mathbf{12}: \\ &0.0023) \gg \mathrm{H_2O\cdots HOH}\ (0.0015) > \mathrm{S\cdots O}\ (\mathbf{8}:\ 0.0013) = \\ &\mathrm{S\cdots O}\ (\mathbf{2}:\ 0.0013) \geq \mathrm{S\cdots O}\ (\mathbf{11}:\ 0.0012) = \mathrm{S\cdots O}\ (\mathbf{5}: \\ &0.0012) > \mathrm{HF\cdots HF}\ (0.0008) = \mathrm{Se\cdots O}\ (\mathbf{10}:\ 0.0008) = \\ &\mathrm{Se\cdots O}\ (\mathbf{4}:\ 0.0008) \geq \mathrm{Se\cdots O}\ (\mathbf{1}:\ 0.0007) \geq \mathrm{Se\cdots O}\ (\mathbf{7}: \\ &0.0006) \gg \mathrm{HCN\cdots HF}\ (-0.0013)\end{aligned} \tag{4}$$

To clarify the relation between $H_b(r_c)$ and $\rho_b(r_c)$ in **1**–**12**, $H_b(r_c)$ was plotted versus $\rho_b(r_c)$ for the compounds given in Equation (3). Figure 6 shows the results. The plots for the hydrogen-bonded and van der Waals adducts are represented by an upward convex curve, shown by the dotted line. The point for NN···HF is very near to the top. While the points for the hydrogen-bonded adducts are on the right-side down slope, those for the van der Waals adducts are on the left-side down slope.[29]

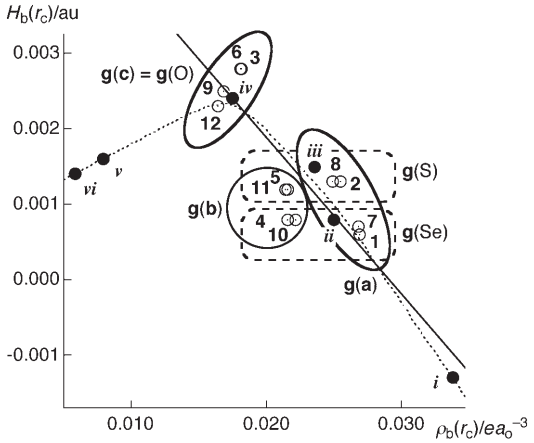

Figure 6. Plots of $H_b(r_c)$ versus $\rho_b(r_c)$ for **1**–**12** as well as hydrogen-bonded (HCN···HF (***i***), HF···HF (***ii***), H_2O···HOH (***iii***), and NN···HF (***iv***)) and van der Waals adducts (Ar···HF (***v***) and Ne···HF (***vi***)). The plot for ***i***–***vi*** is connected by a smooth dotted line. The slope for **1**–**12** and ***i***–***iv*** is shown by a solid line (correlation: $y = -0.21x + 0.0060$; $r = 0.91$). The ATQ system with Z=Se and S construct **g**(**a**) and the 9-MeOATC system with Z=Se and S form **g**(**b**). Groups **g**(**a**) and **g**(**b**) have been reclassified into **g**(Se) and **g**(S). Points for Z=O in both systems belong to **g**(**c**) (=**g**(O)).

The points for **1**–**12** appear along with the dotted line in Figure 6. They form three groups: **g**(**a**), **g**(**b**), and **g**(**c**). Groups **g**(**a**) and **g**(**b**) consist of the ATQ system with Z=Se and S (**1**, **7**, **2**, and **8**) and the 9-MeOATC system with Z=Se and S (**4**, **5**, **10**, and **11**), respectively. On the other hand, the ATQ and 9-MeOATC systems with Z=O (**3**, **6**, **9**, and **12**) belong to **g**(**c**) (=**g**(O)). The points for H_2O···HOH and HF···HF appear very near those in **g**(**a**). Therefore, the nature of the 5c–6e C_2Z_2O and 3c–4e CZO interactions in **g**(**a**) must be similar to hydrogen bonds. This expectation is also supported by the fact that the slope of the points in **g**(**a**) is almost parallel to that of the dotted line. The nature of 5c–6e C_2Z_2O and 3c–4e CZO interactions in **g**(**b**) was analyzed similarly. However, the points for **g**(**c**) are near that of NN···HF, the top of the dotted line, and seem to be on the down slope leading to Ar···HF and Ne···HF. Consequently, it would be difficult to analyze the linear C_2Z_2O and CZO (Z=O) interactions in **g**(**c**) similarly to the cases of **g**(**a**) and **g**(**b**) (Z=Se and S) on the basis of the values of $H_b(r_c)$. Groups **g**(**a**) and **g**(**b**) can be reclassified as **g**(Se) and **g**(S), as shown in Figure 6.

Why is the saturation effect not observed in the formation of 5c–6e C_2Z_2O interactions from a pair of 3c–4e CZO interactions? We noted the bond distances of the compounds predicted by the QC calculations. Shorter Z···O distances were predicted for **1** (2.649 Å) versus **7** (2.652 Å) (Z=Se), **2** (2.626 Å) versus **8** (2.640 Å) (Z=S), and **3** (2.578 Å) versus **9** (2.612 Å) (Z=O) in the ATQ system. The differences increase in the order: Δr(**1**, **7**: −0.003 Å) < Δr(**2**, **8**: −0.014 Å) < Δr(**3**, **9**: −0.034 Å). The smaller distances in 5c–6e C_2Z_2O relative to 3c–4e CZO must operate to prevent saturation. On the other hand, the Z···O distances in the 9-MeOATC system were predicted to be longer in **4** (2.765 Å) versus **10** (2.755 Å) (Z=Se) and in **5** (2.714 Å) versus **11** (2.720 Å) (Z=S). The flexible MeO group at the 9-position must be responsible for the elongation of the bonds.

Figure 7 shows the optimized structures of **4** (**BB**) and **10** (**B**). The larger flip angle for the MeO group at the 9-position of **4** (**BB**), relative to that of **10** (**B**), results in the longer Se···O distance for **4** (**BB**) relative to **10** (**B**). The torsional angle of the O–C_{Me} bond with respect to the ATC plane in **4** (**BB**) is $\varphi(C_1C_9OC_{Me}) = 94.3°$, which is closer to a right angle than in the case of **10** (**B**) (101.7°). The observed structural features in **4** (**BB**) and **10** (**B**) must be controlled

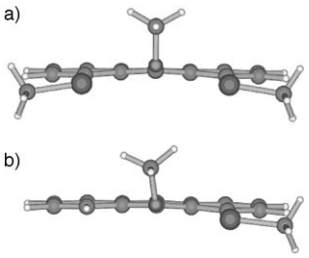

Figure 7. Optimized structures of a) **4** (**BB**) and b) **10** (**B**). The optimized torsional angles ($\varphi(C_1C_9OC_{Me})$) for **4** (**BB**) and **10** (**B**) are 94.3 and 101.7°, respectively.

 © 2007 Wiley-VCH Verlag GmbH & Co. KGaA, Weinheim

by the weak interactions, such as the steric repulsions and attractive interactions in the molecules, which are closely related to the stabilities.

NBO analysis of 5c–6e C_2Z_2O and 3c–4e CZO: How are the 5c–6e C_2Z_2O and 3c–4e CZO interactions stabilized? The second-order perturbation of the NBO analysis[22] was examined for the σ*(C–Z)···n(O)···σ*(Z–C) 5c–6e and n(O)···σ*(Z–C) 3c–4e interactions in the ATQ system of **1**, **2**, **7**, and **8**. The stabilization energy, $E(2)$, associated with the delocalization of the NBO (i)→NBO (j) type, is estimated by Equation (5), in which q_i is the donor orbital occupancy, ε_i and ε_j are the orbital energies of diagonal elements, and $F(i,j)$ is the off-diagonal NBO Fock matrix element. Table 5 shows the results, with the values for 5c–6e C_2Z_2O corresponding to half of the 5c–6e interactions.

$$E(2) = q_i F(i,j)^2/(\varepsilon_j - \varepsilon_i) \quad (5)$$

Table 5. Contributions of donor–acceptor interactions of the n(O)···σ*(Z–C) type in 5c–6e C_2Z_2O and 3c–4e CZO (Z = Se and S) systems.

NBO (i)	NBO (j)	$E(2)$ [kJ mol^{-1}][a]	ΔE [au][b]	$F(i,j)$ [au][c]	Character
1 (**BB**)[d]					
n_p(O)	σ*(Se–C_{Me})	18.5	0.40	0.039	5c–6e
n_s(O)	σ*(Se–C_{Me})	10.6	0.81	0.041	n_s→σ*
2 (**BB**)[e]					
n_p(O)	σ*(S–C_{Me})	13.4	0.45	0.035	5c–6e
n_s(O)	σ*(S–C_{Me})	8.0	0.86	0.031	n_s→σ*
7 (**B**)[f]					
n_p(O)	σ*(Se–C_{Me})	24.6	0.40	0.044	3c–4e
n_s(O)	σ*(Se–C_{Me})	8.0	0.80	0.035	n_s→σ*
8 (**B**)[g]					
n_p(O)	σ*(S–C_{Me})	15.4	0.45	0.037	3c–4e
n_s(O)	σ*(S–C_{Me})	4.4	0.86	0.027	n_s→σ*

[a] Second-order perturbation energy in the NBO analysis. [b] $\Delta E = E(j) - E(i)$. [c] $F(i,j)$ is the off-diagonal NBO Fock matrix element. See Equation (5). [d] ∢C_9OSe = 104.26°, ∢OSeC_{Me} = 173.73°, ∢SeOSe = 151.48°. [e] ∢C_9OS = 101.07°, ∢OSC_{Me} = 179.79°, ∢SOS = 157.85°. [f] ∢C_9OSe = 103.57°, ∢OSeC_{Me} = 173.95°. [g] ∢C_9OS = 99.95°, ∢OSC_{Me} = 179.96°.

Contributions of CT from both n_p(O) and n_s(O) to σ*(Z–C) in **1**, **2**, **7**, and **8** are 58.2, 42.8, 32.6, and 19.8 kJ mol^{-1}, respectively. The values are close to the evaluated energy differences between **BB** and **AA** (or **B** and **A**) for these compounds, which are −49.9, −38.9, −25.5, and −19.7 kJ mol^{-1}, respectively (see Table 6). CT is mainly responsible for ΔE, although the magnitudes of ΔE are smaller than the CT contributions.

Note that n_s(O), as well as n_p(O), contribute much to the σ*(C–Z)···n(O)···σ*(Z–C) 5c–6e and n(O)···σ*(Z–C) 3c–4e interactions. The contributions of n_s(O), relative to n_p(O), are 57, 60, 33, and 29% for **1** (**BB**), **2** (**BB**), **7** (**B**), and **8** (**B**), respectively (Table 5). These ratios must essentially be controlled by ∢ZOC_9 and ∢OZC_{Me}, as well as ∢ZOZ. The ratios for 5c–6e C_2Z_2O (Z = Se and S) are about twice as large as those for 3c–4e CZO (Z = Se and S), respectively. The results show that there is a greater chance of n_s(O) taking part in the σ*(C–Z)···n(O)···σ*(Z–C) interactions with ∢ZOZ = 151–158° than expected based on the 3c–4e CZO interactions.

Energy-lowering effect by 5c–6e C_2Z_2O and 3c–4e CZO: Table 6 collects the energies and selected bond distances and angles optimized for **AA** and **BB** in **1**–**6** and **A** and **B** in **7**, **8**, and **10**.[30]

The energy differences between **BB** and **AA** ($\Delta E(\boldsymbol{n}) = E(\boldsymbol{n}$: **BB**$) - E(\boldsymbol{n}$: **AA**$)$, where n = 1–6) were examined. The values of ΔE(**1**), ΔE(**2**), ΔE(**4**), and ΔE(**5**) are −49.9, −38.9, −33.1, and −25.2 kJ mol^{-1}, respectively. The differences must be a reflection of the stabilization in 5c–6e C_2S_2O relative to 5c–6e C_2Se_2O and the p–π conjugation of n_p(Se)–π(ATQ) type versus that of n_p(Se)–π(ATC) type. The ratios of ΔE(**2**)/ΔE(**1**) and ΔE(**5**)/ΔE(**4**) are 0.76–0.78, which shows that the energy-lowering effect of the 5c–6e C_2S_2O interaction is about three quarters that of 5c–6e C_2Se_2O if the system is the same. The ratios of ΔE(**4**)/ΔE(**1**) and ΔE(**5**)/ΔE(**2**) are 0.65–0.66. The effect on the 9-MeOATC system is about two thirds of that on the ATQ system if Z is the same.[31]

The nonbonded Z···O distances in **BB** are shorter than those in **AA** ($\Delta r(\boldsymbol{n}) = r(\boldsymbol{n}$: **BB**$) - r(\boldsymbol{n}$: **AA**$) < 0$, for n = 1–6). The values of Δr(**1**), Δr(**2**), Δr(**4**), and Δr(**5**) are −0.336, −0.308, −0.270, and −0.239 Å, respectively. The large steric repulsion in **AA** must be reduced by the longer r(**AA**). On the other hand, the enlarged steric repulsion caused by the shorter r(**BB**) would be compensated by the energy-lowering effect through the formation of a 5c–6e C_2Z_2O interaction, together with p–π conjugation.

The energy differences between **B** and **A** ($\Delta E(\boldsymbol{n}) = E(\boldsymbol{n}$: **B**$) - E(\boldsymbol{n}$: **A**$)$, where n = 7, 8, and 10) were also examined. The ΔE(**7**), ΔE(**8**), and ΔE(**10**) values are −25.5, −19.7, and −10.8 kJ mol^{-1}, respectively. Whereas the ΔE(**1**) and ΔE(**2**) values are nearly twice as large as ΔE(**7**) and ΔE(**8**), respectively, ΔE(**4**) is about three times as large as ΔE(**10**). The flexibility around the MeO group must be responsible for these predictions (see Figure 7). The σ*(C–Z)←n_p(O)→σ*(Z–C) 5c–6e interaction is demonstrated to operate effectively by the connection of two n_p(O)→σ*(Z–C) 3c–4e interactions through the central n_p(O) orbital in the ATQ and 9-MeOATC systems with Z = Se and S, although n_s(O) also contributes to the interactions.

Scheme for the formation of 5c–6e C_2Z_2O interactions: Extended hypervalent 5c–6e C_2Z_2O interactions of the σ*(C–Z)···n_p(O)···σ*(Z–C) type will form when two hypervalent

 © 2007 Wiley-VCH Verlag GmbH & Co. KGaA, Weinheim

Table 6. Energies, together with the selected bond lengths, angles, and torsional angles, optimized for **AA** and **BB** in **1–6** and **A** and **B** in **7**, **8**, and **10**.[a]

Compound	E [au]	ΔE [kJ mol^{-1}]	$r(C_i–Z)$ [Å]	$r(Z–C_{Me})$ [Å]	$r(O\cdots Z)$ [Å]	$\Delta r(O\cdots Z)$ [Å]	$\sphericalangle C_iZC_{Me}$	$\sphericalangle OZC_{Me}$	$\sphericalangle ZOZ$	$\phi(C_iC_1ZC_{Me})$
1 (BB)	−5570.7164	−49.9	1.9198	1.9716	2.6493	−0.3361	99.71	173.73	151.48	180.00
1 (AA)	−5570.6974	0.0	1.9358	1.9622	2.9854	0.0000	103.80	68.66	157.50	58.39
2 (BB)	−1564.0561	−38.9	1.7724	1.8232	2.6258	−0.3081	102.69	179.79	157.85	180.00
2 (AA)	−1564.0413	0.0	1.7847	1.8211	2.9339	0.0000	105.75	70.49	163.19	60.01
3 (BB)	−918.0790	−13.7	1.3454	1.4187	2.5775	−0.1307	119.84	151.62	179.46	180.00
3 (AA)	−918.0738	0.0	1.3618	1.4300	2.7082	0.0000	117.12	84.13	179.24	80.29
4 (BB)	−5535.9609	−33.1	1.9350	1.9623	2.7651	−0.2699	100.23	172.38	143.74	−176.25
4 (AA)	−5535.9483	0.0	1.9451	1.9639	3.0350	0.0000	100.45	76.70	154.52	65.76
5 (BB)	−1529.3040	−25.2	1.7847	1.8163	2.7137	−0.2389	103.07	175.12	150.10	−177.82
5 (AA)	−1529.2944	0.0	1.7948	1.8228	2.9526	0.0000	102.78	77.93	159.03	67.82
6 (BB)	−883.3365	−17.3	1.3572	1.4161	2.5783	−0.1043	119.06	151.01	176.60	−177.68
6 (AA)	−883.3299	0.0	1.3748	1.4266	2.6826	0.0000	115.32	88.81	177.72	86.75
7 (B)	−3129.8466	−25.5	1.9189	1.9716	2.6518	−0.3660	99.64	173.95	–	180.00
7 (A)	−3129.8369	0.0	1.9377	1.9630	3.0178	0.0000	103.32	68.87	–	62.19
8 (B)	−1126.5164	−19.7	1.7713	1.8229	2.6398	−0.3460	102.67	179.96	–	180.00
8 (A)	−1126.5089	0.0	1.7832	1.8208	2.9858	0.0000	105.99	69.20	–	57.66
10 (B)	−3095.0962	−10.8	1.9345	1.9629	2.7545	−0.3001	100.16	173.40	–	178.81
10 (A)	−3095.0921	0.0	1.9436	1.9663	3.0546	0.0000	100.50	73.74	–	63.69

[a] Optimized with the 6-311+G(2df) basis set for oxygen and Z (Z=Se, S, and O) atoms and the 6-311+G(2d,p) basis set for carbon and hydrogen atoms at the DFT (B3LYP) level of the Gaussian 03 program.

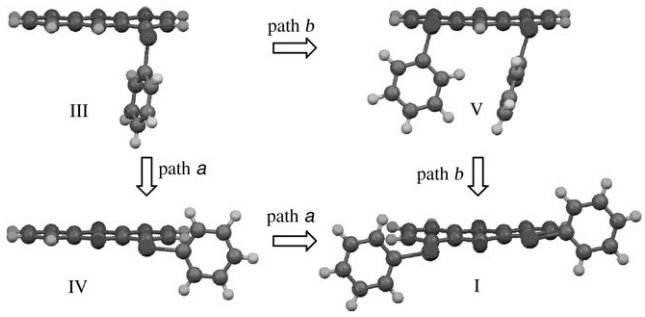

Scheme 4. Formation of 5c–6e C_2Se_2O starting from 1c–2e n_p(Se), exemplified by phenylselanyl derivatives.

3c–4e CZO interactions are connected effectively through the central n_p(O) orbital, as shown in Scheme 3. Scheme 4 shows a scheme for the formation of 5c–6e C_2Se_2O interactions, as exemplified by the formation of **I**,[3] starting from the n_p(Se) orbital (1c–2e) in 1-(phenylselanyl)anthracene (**III**).[32] Path *a* shows a process via 1-(phenylselanyl)anthraquinone (**IV**)[33] and path *b* a process via 1,8-bis(phenylselanyl)anthracene (**V**).[3]

When the two hydrogen atoms at the 9,10-positions in **III** are replaced by carbonyl oxygen atoms in path *a*, **III** (**A**) changes to **IV** (**B**) with the formation of 3c–4e CSeO interactions.[33] Anthraquinone **I** (**BB**) forms if the hydrogen atom at the 8-position of **IV** (**B**) is then substituted by a PhSe group in path *a*. The 3c–4e CSeO interaction in **IV** (**B**) changes to a 5c–6e C_2Se_2O interaction in this substitution with two Se–C_{Ph} bonds and an oxygen atom at the 1,8,9-positions of **I** (**BB**). On the other hand, anthracene **III** (**A**) with a n_p(Se) orbital (1c–2e) is transformed to **V** (**AA**) with two independent n_p(Se) orbitals (a couple of 1c–2e) in path *b* when the hydrogen atom at the 8-position in **III** (**A**) is substituted by another PhSe group. Anthracene **V** (**AA**) changes to **I** (**BB**) by replacement of the hydrogen atoms at the 9,10-positions in **V** (**AA**) with carbonyl oxygen atoms. In this process, the two independent n_p(Se) orbitals (a pair of independent 1c–2e) in **V** (**AA**) are incorporated into the 5c–6e C_2Se_2O interaction in **I** (**BB**). A similar scheme can be drawn for **II**.

AIM analysis of **1–12** revealed the nature of C–Z···O···Z–C 5c–6e (Z=Se, S, and O) and C–Z···O 3c–4e interactions. NBO analysis and the energies calculated for **1–12** support the discussion. The structural change from **III** (**A**) to **I** (**BB**) in Scheme 4 shows how 5c–6e C_2Se_2O interactions are constructed from a n_p(Se) orbital (1c–2e) through 3c–4e CSeO interactions or two independent n_p(Se) orbitals (a pair of independent 1c–2e).

Conclusion

The nature of BCPs in the $n_p(O)\cdots\sigma^*(Z–C)$ interactions (Z=Se, S, and O) in **1–12** has been examined by using the AIM method after determination of the structures of **1–3** by

 © 2007 Wiley-VCH Verlag GmbH & Co. KGaA, Weinheim

means of X-ray crystallographic analysis. The $\rho_b(r_c)$ values of the $n_p(O)\cdots\sigma^*(Z-C)$ interactions (Z = Se, S, and O) in **1**–**12** are summarized in Equations (1)–(3). The $\rho_b(r_c)$ and $\nabla^2\rho_b(r_c)$ values of the BCPs in the nonbonded Z···O···Z interactions in **1**–**6** are, respectively, very close to those corresponding to the O···Z interactions in **7**–**12**. Consequently, the two $n_p(O)\cdots\sigma^*(Z-C)$ interactions in **1**–**6** have been demonstrated to be connected effectively at the central $n_p(O)$ orbital to form extended hypervalent 5c–6e interactions of the $\sigma^*(C-Z)\cdots n_p(O)\cdots\sigma^*(Z-C)$ type. The direction of the CT is of $\sigma^*(C-Z)\leftarrow n_p(O)\rightarrow\sigma^*(Z-C)$ type. The $H_b(r_c)$ term was also applied to the 5c–6e C_2Z_2O and 3c–4e CZO systems in **1**–**12**, which must be a more appropriate index of weak interactions. The results emphasize that the strength of the interactions increase in the order: O···O ≪ S···O < Se···O.

The contributions of CT to 5c–6e C_2Z_2O and 3c–4e CZO were evaluated by using NBO analysis. The results have been related to the energy differences between structures **BB** and **AA**, which were also calculated. The ΔE(**1**) value (= E(**1**: **BB**) − E(**1**: **AA**)) is −49.9 kJ mol^{-1}, ΔE(**2**) = −38.9 kJ mol^{-1}, ΔE(**4**) = −33.1 kJ mol^{-1}, and ΔE(**5**) = −25.2 kJ mol^{-1}. The differences must reflect the stabilization of 5c–6e C_2S_2O relative to 5c–6e C_2Se_2O and the p–π conjugation of the $n_p(Se)$–π(ATQ) type versus that of the $n_p(Se)$–π(ATC) type. The ratios of ΔE(**2**)/ΔE(**1**) and ΔE(**5**)/ΔE(**4**) are 0.76–0.78, which shows that the energy-lowering effect of 5c–6e C_2S_2O is about three quarters that of 5c–6e C_2Se_2O, if the system is the same. The ratios of ΔE(**4**)/ΔE(**1**) and ΔE(**5**)/ΔE(**2**) are 0.65–0.66, which shows that the effect in the 9-MeOATC system is about two thirds that in the ATQ group, if Z is the same. Nonbonded Z···O distances were also examined: r(**AA**) is longer than the corresponding r(**BB**) distance in **1**–**6**. The large steric repulsion must be reduced in **AA** by the longer r(**AA**) and the increased steric repulsion caused by the shorter r(**BB**) would be compensated by the energy-lowering effect through the formation of 5c–6e C_2Z_2O as well as the p–π conjugation.

The structures of the phenylselanyl derivatives of ATQ provide a scheme detailing the formation of the 5c–6e C_2Se_2O system, starting from $n_p(Se)$ (1c–2e), by two pathways. One is by way of the 3c–4e CSeO system and the other is through two independent $n_p(Se)$ orbitals (a pair of independent 1c–2e). The scheme clarifies how weak interactions such as 5c–6e C_2Se_2O determine the fine structures of compounds.

Experimental Section

General: Manipulations were performed under nitrogen or argon using standard vacuum-line techniques. Glassware was dried at 130 °C overnight. Solvents and reagents were purified by standard procedures as necessary. Melting points were measured with a Yanako MP-S3 and uncorrected. NMR spectra were recorded at 25 °C with a JEOL JNM-AL 300 spectrometer (^{1}H, 300 MHz; ^{13}C, 75.45 MHz; ^{77}Se, 57.25 MHz). The ^{1}H, ^{13}C, and ^{77}Se chemical shifts are given in parts per million relative to those of Me_4Si, internal $CDCl_3$, and external MeSeMe, respectively. Column chromatography was performed on silica gel (Fuji Silysia BW-300) and acidic and basic alumina (E. Merk). Flash column chromatography was performed with 300—400 mesh silica gel and acidic and basic alumina. Analytical thin-layer chromatography was performed on precoated silica gel plates (60F-254) using the systems (v/v) indicated. Elemental analyses were performed by using a J-Science Lab Co., Ltd., JM10 Micro Corder.

1,8-Bis(methylselanyl)anthraquinone (1): A suspension of dimethyl diselenide (1.00 g, 5.32 mmol) and sodium hydride (0.49 g, 12.77 mmol) in dry DMF (60 mL) was heated at 110 °C for 1 h. Then 1,8-dibromoanthraquinone (1.47 g, 5.32 mmol) and CuI (2.33 g, 12.23 mmol) were added to the solution at 110 °C. After stirring for 3 h at 140 °C, the solution was subjected to dry chromatography on silica gel (dichloromethane as eluent) and concentrated under vacuo. The product was purified by using chromatography on silica gel (benzene as eluent) and recrystallized from benzene/ethanol. Compound **1** was obtained as a red solid (0.12 g, 5.7 % yield). M.p. 267.5–268.9 °C; ^{1}H NMR (300.40 MHz, $CDCl_3$/TMS): δ = 2.53 (s, 6H; CH_3Se), 7.62–7.71 (m, 4H), 8.08 ppm (dd, ^3J(H,H) = 6.8 Hz, ^4J(H,H) = 1.7 Hz, 2H); ^{13}C NMR (74.45 MHz, $CDCl_3$/TMS): δ = 65.7 (*C*H$_3$Se), 124.0, 130.7, 132.6, 132.6, 134.8, 141.8, 183.1 (C=O), 184.2 ppm (C=O); ^{77}Se NMR (57.25 MHz, $CDCl_3$/MeSeMe): δ = 315.7 ppm; elemental analysis calcd (%) for $C_{16}H_{12}O_2Se_2$: C 48.75, H 3.07; found: C 48.75, H 3.17.

1,8-Bis(methylthio)anthraquinone (2): Following a method similar to that for **1**, compound **2** was obtained as orange needles (0.28 g, 23 % yield). M.p. 234.5–235.8 °C; ^{1}H NMR (300.40 MHz, $CDCl_3$/TMS): δ = 2.32 (s, 6H; CH_3S), 7.65 (t, ^3J(H,H) = 7.7 Hz, 2H), 7.77 (d, ^3J(H,H) = 7.9 Hz, 2H), 8.15 ppm (dd, ^3J(H,H) = 7.4 Hz, ^4J(H,H) = 1.2 Hz, 2H); ^{13}C NMR (74.45 MHz, $CDCl_3$/TMS): δ = 65.6 (*C*H$_3$S), 122.8, 129.2, 129.5, 132.6, 134.2, 145.9, 183.2 (C=O), 184.1 ppm (C=O); elemental analysis calcd (%) for $C_{16}H_{12}O_2S_2$: C 63.97, H 4.03; found: C 63.85, H 4.13.

1,8-Bis(methoxy)anthraquinone (3):[34] Sodium hydride (0.83 g, 21.68 mmol) was added to a solution of chrysazin (2.00 g, 8.33 mmol) in a mixture of dry THF (40 mL) and dry DMF (20 mL). The solution was stirred for 30 min and then left at reflux for 30 min. Methyl iodide (1.56 mL, 24.98 mmol) was added to the solution cooled to room temperature. Then the solution was stirred for 2 h at this temperature. As the reaction was initiated by heating, methyl iodide (1.56 mL, 24.98 mmol) was added to the solution at 60 °C. After cooling to 25 °C, sodium hydride (0.45 g, 11.62 mmol) was added. The reaction mixture was left at reflux for 30 min, stirred at room temperature overnight, and then concentrated. The crude product was purified by using chromatography on silica gel (dichloromethane as eluent) and recrystallized from benzene/ethanol. Compound **3** was obtained as yellow needles (1.79 g, 78 % yield). M.p. 225.8–226.8 °C; ^{1}H NMR (300.40 MHz, $CDCl_3$/TMS): δ = 4.01 (s, 6H; CH_3O), 7.30 (d, ^3J(H,H) = 8.3 Hz, 2H), 7.63 (t, ^3J(H,H) = 8.1 Hz, 2H), 7.83 ppm (d, ^3J(H,H) = 7.5 Hz, 2H); ^{13}C NMR (74.45 MHz, $CDCl_3$/TMS): δ = 56.5 (CH_3O), 118.0, 118.8, 123.9, 133.8, 134.7, 159.4, 182.8 (C=O), 184.0 ppm (C=O); elemental analysis calcd (%) for $C_{16}H_{12}O_4$: C 71.64, H 4.51; found: C 71.62, H 4.54.

X-ray structure determination: Single crystals of red prisms of **1**, orange needles of **2**, and yellow needles of **3** were obtained by slow evaporation of solutions of the compounds dissolved in benzene containing ethanol. X-ray diffraction data for **1**–**3** were collected on a Rigaku/MSC Mercury CCD diffractometer equipped with a graphite-monochromated $Mo_{K\alpha}$ radiation source (λ = 0.71070 Å) at 103(2) K. The structures of **1**–**3** were solved by direct methods (SIR97),[35] and refined by the full-matrix least-squares method on F^2 for all reflections (SHELXL-97).[36] All non-hydrogen atoms were refined anisotropically; hydrogen atoms were refined isotropically.

CCDC-603371 (**1**), CCDC-603372 (**2**), and CCDC-603373 (**3**) contain the supplementary crystallographic data for this paper. These data can be obtained free of charge from the Cambridge Crystallographic Data Centre via www.ccdc.cam.ac.uk/data_request/cif.

MO calculations: Ab initio molecular orbital calculations were performed on a Silent-SCC T2 (Itanium2) computer by employing the Gaussian 03 program[20] with the 6-311+G(2df) basis set for oxygen, sulfur, and selenium atoms and the 6-311+G(2d,p) basis set for carbon and hydrogen atoms. Calculations were performed on structures **BB** and **AA** of

 © 2007 Wiley-VCH Verlag GmbH & Co. KGaA, Weinheim

1–**6**, structure **B** of **7**–**12**, and structure **A** of **7**, **8**, and **10** at the density functional theory (DFT) level of the Becke three-parameter hybrid functional combined with the Lee–Yang–Parr correlation functional (B3LYP). AIM analysis was performed with the AIM2000 program[20] after optimization of the structures.

Acknowledgements

This work was partially supported by a Grant-in-Aid for Scientific Research (No. 16550038) from the Ministry of Education, Culture, Sports, Science, and Technology, Japan.

[1] a) J. C. Martin, M. M. Chau, *J. Am. Chem. Soc.* **1974**, *96*, 3319–3321; b) S. Alvarez, F. Mota, J. Novoa, *J. Am. Chem. Soc.* **1987**, *109*, 6586–6591; c) W. B. Farnham, D. A. Dixon, J. C. Calabrese, *J. Am. Chem. Soc.* **1988**, *110*, 8453–8461; d) W. Nakanishi, "Hypervalent Chalcogen Compounds" in *Handbook of Chalcogen Chemistry: New Perspectives in Sulfur, Selenium and Tellurium* (Ed.: F. A. Devillanova), Royal Society of Chemistry, Cambridge, Chapter 10.3, **2006**, in press.

[2] a) W. Nakanishi, S. Hayashi, S. Toyota, *Chem. Commun.* **1996**, 371–372; b) W. Nakanishi, S. Hayashi, S. Toyota, *J. Org. Chem.* **1998**, *63*, 8790–8800; c) W. Nakanishi, S. Hayashi, T. Arai, *Chem. Commun.* **2002**, 2416–2417.

[3] a) W. Nakanishi, S. Hayashi, N. Itoh, *Chem. Commun.* **2003**, 124–125; b) W. Nakanishi, S. Hayashi, N. Itoh, *J. Org. Chem.* **2004**, *69*, 1676–1684; c) W. Nakanishi, S. Hayashi, T. Furuta, N. Itoh, Y. Nishina, M. Yamashita, Y. Yamamoto, *Phosphorus Sulfur Silicon Relat. Elem.* **2005**, *180*, 1351–1355.

[4] W. Nakanishi, S. Hayashi, S. Yamaguchi, K. Tamao, *Chem. Commun.* **2004**, 140–141.

[5] a) G. C. Pimentel, *J. Chem. Phys.* **1951**, *19*, 446–448; b) J. I. Musher, *Angew. Chem.* **1969**, *81*, 68–83; *Angew. Chem. Int. Ed. Engl.* **1969**, *8*, 54–68; c) R. J. Hatch, R. E. Rundle, *J. Am. Chem. Soc.* **1951**, *73*, 4321–4324; d) R. E. Rundle, *J. Am. Chem. Soc.* **1963**, *85*, 112–113.

[6] a) M. M. L. Chen, R. Hoffmann, *J. Am. Chem. Soc.* **1976**, *98*, 1647–1653; b) P. J. Hay, *J. Am. Chem. Soc.* **1977**, *99*, 1003–1012; c) W. Kutzelnigg, *Angew. Chem.* **1984**, *96*, 262–286; *Angew. Chem. Int. Ed. Engl.* **1984**, *23*, 272–295; d) A. E. Reed, F. Weinhold, *J. Am. Chem. Soc.* **1986**, *108*, 3586–3593; e) A. E. Reed, P. von R. Schleyer, *J. Am. Chem. Soc.* **1990**, *112*, 1434–1445; f) M. M. L. Chen, R. Hoffmann, *J. Am. Chem. Soc.* **1976**, *98*, 1647–1653; g) P. A. Cahill, C. E. Dykstra, J. C. Martin, *J. Am. Chem. Soc.* **1985**, *107*, 6359–6362; h) N. C. Baenziger, R. E. Buckles, R. J. Maner, T. D. Simpson, *J. Am. Chem. Soc.* **1969**, *91*, 5749–5755.

[7] a) R. A. Hayes, J. C. Martin, "Sulfurane Chemistry" in *Organic Sulfur Chemistry: Theoretical and Experimental Advances* (Eds.: F. Bernardi, I. G. Csizmadia, A. Mangini), Elsevier, Amsterdam, **1985**, Chapter 8; b) J. Bergman, L. Engman, J. Siden, "Tetra- and Higher-Valent (Hypervalent) Derivatives of Selenium and Tellurium" in *The Chemistry of Organic Selenium and Tellurium Compounds, Vol. 1* (Eds.: S. Patai, Z. Rappoport), Wiley, New York, **1986**, Chapter 14; c) *The Organic Chemistry of Tellurium* (Ed.: K. J. Irgolic), Gordon and Breach, New York, **1974**.

[8] *Chemistry of Hypervalent Compounds* (Ed.: K.-y. Akiba), Wiley-VCH, New York, **1999**.

[9] a) G. Mugesh, A. Panda, H. B. Singh, N. S. Punekar, R. J. Butcher, *Chem. Commun.* **1998**, 2227–2228; b) J. E. Drake, M. B. Hursthouse, M. Kulcsar, M. E. Light, A. Silvestru, *Phosphorus Sulfur Silicon* **2001**, *169*, 293–296; c) G. Mugesh, A. Panda, H. B. Singh, N. S. Punekar, R. J. Butcher, *J. Am. Chem. Soc.* **2001**, *123*, 839–850; d) S. Tomoda, M. Iwaoka, *J. Chem. Soc., Chem. Commun.* **1990**, 231–233; e) J. E. Drake, M. B. Hursthouse, M. Kulcsar, M. E. Light, A. Silvestru, *J. Organomet. Chem.* **2001**, *623*, 153–160; f) G. Mugesh, A. Panda, S. Kumar, S. D. Apte, H. B. Singh, R. J. Butcher, *Organometallics* **2002**, *21*, 884–892; g) J. R. Anacona, J. Gomez, D. Lorono, *Acta Crystallogr., Sect. C* **2003**, *59*, o277–o280; h) G. Mugesh, H. B. Singh, R. J. Butcher, *Eur. J. Inorg. Chem.* **1999**, 1229–1236; i) R. Kaur, H. B. Singh, R. P. Patel, *J. Chem. Soc., Dalton Trans.* **1996**, 2719–2726; j) G. Mugesh, H. B. Singh, R. J. Butcher, *J. Organomet. Chem.* **1999**, *577*, 243–248; see also, k) D. Shimizu, N. Takeda, N. Tokitoh, *Chem. Commun.* **2006**, 177–178.

[10] a) *Atoms in Molecules. A Quantum Theory* (Ed.: R. F. W. Bader), Oxford University Press, Oxford, **1990**; b) R. F. W. Bader, T. S. Slee, D. Cremer, E. Kraka, *J. Am. Chem. Soc.* **1983**, *105*, 5061–5068; c) R. F. W. Bader, *Chem. Rev.* **1991**, *91*, 893–926; d) R. F. W. Bader, *J. Phys. Chem. A* **1998**, *102*, 7314–7323; e) F. W. Biegler-König, R. F. W. Bader, T. H. Tang, *J. Comput. Chem.* **1982**, *3*, 317–328; f) R. F. W. Bader, *Acc. Chem. Res.* **1985**, *18*, 9–15; g) T. H. Tang, R. F. W. Bader, P. MacDougall, *Inorg. Chem.* **1985**, *24*, 2047–2053; h) F. Biegler-König, J. Schönbohm, D. Bayles, *J. Comput. Chem.* **2001**, *22*, 545–559; i) F. Biegler-König, J. Schönbohm, *J. Comput. Chem.* **2002**, *23*, 1489–1494.

[11] J. Molina, J. A. Dobado, *Theor. Chem. Acc.* **2001**, *105*, 328–337.

[12] J. A. Dobado, H. Martinez-Garcia, J. Molina, M. R. Sundberg, *J. Am. Chem. Soc.* **2000**, *122*, 1144–1149.

[13] a) M. Yamashita, Y. Yamamoto, K.-y. Akiba, D. Hashizume, F. Iwasaki, N. Takagi, S. Nagase, *J. Am. Chem. Soc.* **2005**, *127*, 4354–4371; b) Y. Yamamoto, K.-y. Akiba, *Yuki Gosei Kagaku Kyokaishi* **2004**, *62*, 1128–1137.

[14] S. K. Ignatov, N. H. Rees, B. R. Tyrrell, S. R. Dubberley, A. G. Razuvaev, P. Mountford, G. I. Nikonov, *Chem. Eur. J.* **2004**, *10*, 4991–4999.

[15] H. M. Muchall, *ARKIVOC* **2001**, *7*, 82–86.

[16] S. K. Tripathi, U. Patel, D. Roy, R. B. Sunoj, H. B. Singh, G. Wolmershäuser, R. J. Butcher, *J. Org. Chem.* **2005**, *70*, 9237–9247.

[17] Structures of the naphthalene system 8-G-1-(ArSe)$C_{10}H_6$ are well classified by type **A** (**A**), type **B** (**B**), and type **C** (**C**) structures, with the Se–C_{Ar} bond located almost perpendicular to the naphthyl plane in **A** and in the naphthyl plane in **B**, whereas **C** is a structure intermediate between **A** and **B** (see ref. [38] and also Scheme 2).

[18] A. Bondi, *J. Phys. Chem.* **1964**, *68*, 441–451.

[19] The nonbonded O···S distances in **2** (S-B) are 2.6495(11) and 2.6392(11) Å. The O(1B)–S(1B)–C(15B) and O(1B)–S(2B)–C(16B) angles in **2** (S-B) are 178.49(5) and 171.98(6)°, respectively. The S(1B)–O(1B)–S(2B) angle is 157.97(4)°.

[20] Gaussian 03, Revision B.05, M. J. Frisch, G. W. Trucks, H. B. Schlegel, G. E. Scuseria, M. A. Robb, J. R. Cheeseman, J. A. Montgomery, Jr., T. Vreven, K. N. Kudin, J. C. Burant, J. M. Millam, S. S. Iyengar, J. Tomasi, V. Barone, B. Mennucci, M. Cossi, G. Scalmani, N. Rega, G. A. Petersson, H. Nakatsuji, M. Hada, M. Ehara, K. Toyota, R. Fukuda, J. Hasegawa, M. Ishida, T. Nakajima, Y. Honda, O. Kitao, H. Nakai, M. Klene, X. Li, J. E. Knox, H. P. Hratchian, J. B. Cross, V. Bakken, C. Adamo, J. Jaramillo, R. Gomperts, R. E. Stratmann, O. Yazyev, A. J. Austin, R. Cammi, C. Pomelli, J. W. Ochterski, P. Y. Ayala, K. Morokuma, G. A. Voth, P. Salvador, J. J. Dannenberg, V. G. Zakrzewski, S. Dapprich, A. D. Daniels, M. C. Strain, O. Farkas, D. K. Malick, A. D. Rabuck, K. Raghavachari, J. B. Foresman, J. V. Ortiz, Q. Cui, A. G. Baboul, S. Clifford, J. Cioslowski, B. B. Stefanov, G. Liu, A. Liashenko, P. Piskorz, I. Komaromi, R. L. Martin, D. J. Fox, T. Keith, M. A. Al-Laham, C. Y. Peng, A. Nanayakkara, M. Challacombe, P. M. W. Gill, B. Johnson, W. Chen, M. W. Wong, C. Gonzalez, J. A. Pople, Gaussian, Inc., Wallingford CT, **2004**.

[21] AIM2000 program (version 2.0) employed to analyze and visualize atoms in molecules: F. W. Biegler-König, J. Schönbohm, D. Bayles, *J. Comput. Chem.* unpublished results.

[22] NBO (version 3.1), E. D. Glendening, A. E. Reed, J. E. Carpenter, F. Weinhold, Theoretical Chemistry Institute, University of Wisconsin, Madison, **2001**.

[23] The MP2 level with the same basis sets also gave similar results (see Table 4).

[24] Contributions of π(C=O) character to **7** and **8** are also predicted to be very small ($\lambda_1/\lambda_2-1=0.07$ for both). The ionic C^+-O^- nature of

 © 2007 Wiley-VCH Verlag GmbH & Co. KGaA, Weinheim

the C=O bond must be very large, as the (Qn(C), Qn(O)) values are (0.552, −0.565) for **7** and (0.551, −0.558) for **8**.

[25] The energies of the structures with C_{2v} symmetry are slightly lower than those with C_2 symmetry for **1**–**3**.

[26] Two factors may operate to determine the conformation of the MeO group in the 1,8-positions of the anthracene **13**. One is the energy-lowering effect by CT in the O···B···O interaction: the n_p(O) orbital must be more effective for CT, which requires the OMe groups to adopt the **AA** conformation. Another factor is the p–π conjugation of n(O)–π(ATC) type, which places the groups in the ATC plane (the **BB** conformation). If the p–π conjugation contributes more than CT, the OMe groups will adopt the **BB** conformation. The **BB** structure of **13** shows that the p–π conjugation does indeed contribute more than CT to **13**, although the crystal-packing effect must also be considered.

[27] The $\rho_b(r_c)$ value was reported to be 0.022 $e a_o^{-3}$ for [9-$(MeO)_2$C-1,8-$(MeO)_2C_{14}H_7]^+$ (see ref. [13a]).

[28] a) E. Espinosa, E. Molins, C. Lecomte. *Chem. Phys. Lett.* **1998**, *285*, 170–173; b) E. Espinosa, M. Souhassou, H. Lachekar, C. Lecomte, *Acta Crystallogr., Sect. B* **1999**, *55*, 563–572; c) E. Espinosa, C. Lecomte, E. Molins, *Chem. Phys. Lett.* **1999**, *300*, 745–748; d) E. Espinosa, I. Alkorta, I. Rozas, J. Elguero, E. Molins, *Chem. Phys. Lett.* **2001**, *336*, 457–461; e) C, Gatti, L. Bertini, *Acta Crystallogr. Sect. A* **2004**, *60*, 438–449.

[29] The reasons for the variation in values of $H_b(r_c)$ of the hydrogen-bonded and van der Waals adducts, as well as **g**(O), in the plots in Figure 6 are of interest. Studies are in progress and will be discussed elsewhere.

[30] The 5c–6e interactions in **1**, **2**, **4**, and **5** are well demonstrated based on the molecular orbitals, although not shown (cf. Scheme 1). MolStudio R3.2, Rev. 1.0, NEC Corporation, **1997**–**2003**.

[31] ΔE(**I**) and ΔE(**II**) are −60.6 and −36.5 kJ mol^{-1}, respectively (ΔE(**II**)/ΔE(**I**) = 0.60) (see ref. [3]). The values are larger than ΔE(**1**) and ΔE(**4**), respectively, although the basis sets for the calculations are not the same.

[32] The structure of **III** was determined by means of X-ray crystallographic analysis: W. Nakanishi S. Hayashi, unpublished results.

[33] W. Nakanishi, S. Hayashi, D. Shimizu, M. Hada, *Chem. Eur. J.* **2006**, *12*, 3829–3846.

[34] H. Quast, H.-L. Fuchsbauer, *Chem. Ber.* **1986**, *119*, 2414–2429.

[35] A. Altomare, M. C. Burla, M. Camalli, G. L. Cascarano, C. Giacovazzo, A. Guagliardi, A. G. G. Moliterni, G. Polidori, R. Spagna, *J. Appl. Crystallogr.* **1999**, *32*, 115–119.

[36] SHELXL-97, Program for the Refinement of Crystal Structures, G. M. Sheldrick, University of Göttingen, Göttingen, **1997**.

[37] Gaussian 98 (Revision A.9), M. J. Frisch, G. W. Trucks, H. B. Schlegel, G. E. Scuseria, M. A. Robb, J. R. Cheeseman, V. G. Zakrzewski, J. A. Montgomery, R. E. Stratmann, J. C. Burant, S. Dapprich, J. M. Millam, A. D. Daniels, K. N. Kudin, M. C. Strain, O. Farkas, J. Tomasi, V. Barone, M. Cossi, R. Cammi, B. Mennucci, C. Pomelli, C. Adamo, S. Clifford, J. Ochterski, G. A. Petersson, P. Y. Ayala, Q. Cui, K. Morokuma, D. K. Malick, A. D. Rabuck, K. Raghavachari, J. B. Foresman, J. Cioslowski, J. V. Ortiz, A. G. Baboul, B. B. Stefanov, G. Liu, A. Liashenko, P. Piskorz, I. Komaromi, R. Gomperts, R. L. Martin, D. J. Fox, T. Keith, M. A. Al-Laham, C. Y. Peng, A. Nanayakkara, C. Gonzalez, M. Challacombe, P. M. W. Gill, B. G. Johnson, W. Chen, M. W. Wong, J. L. Andres, M. Head-Gordon, E. S. Replogle, J. A. Pople, Gaussian, Inc., Pittsburgh, PA, **1998**.

[38] a) W. Nakanishi, S. Hayashi, T. Uehara, *Eur. J. Org. Chem.* **2001**, *2001*, 3933–3943; b) S. Hayashi, W. Nakanishi, *J. Org. Chem.* **1999**, *64*, 6688–6696; c) W. Nakanishi, S. Hayashi, H. Yamaguchi, *Chem. Lett.* **1996**, 947–948; d) W. Nakanishi, S. Hayashi, A. Sakaue, G. Ono, Y. Kawada, *J. Am. Chem. Soc.* **1998**, *120*, 3635–3640; e) W. Nakanishi, S. Hayashi, *J. Org. Chem.* **2002**, *67*, 38–48; f) W. Nakanishi, S. Hayashi, T. Uehara, *J. Phys. Chem. A* **1999**, *103*, 9906–9912.

Received: April 4, 2006
Revised: July 25, 2006
Published online: October 26, 2006

Please note: Minor changes have been made to this manuscript since its publication in *Chemistry—A European Journal* Early View. The Editor.

 © 2007 Wiley-VCH Verlag GmbH & Co. KGaA, Weinheim